RESEARCH ARTICLE

VOLCANICA

Conduit formation and crustal microxenolith entrainment in a basaltic fissure eruption: Observations from Thríhnúkagígur Volcano, Iceland

 Michael R. Hudak*[α,β], Maureen D. Feineman[α], Peter C. LaFemina[α], Halldór Geirsson[α,γ], and Samuele Agostini[δ]

[α] Department of Geosciences, The Pennsylvania State University, University Park, PA 16802.
[β] Marine Chemistry and Geochemistry, Woods Hole Oceanographic Institution, Woods Hole, MA 02543.
[γ] Nordic Volcanological Center, Institute of Earth Sciences, University of Iceland, IS-101, University of Iceland, Reykjavík, Iceland.
[δ] Istituto di Geoscienze e Georisorse, Consiglio Nazionale delle Ricerche, Pisa, Italy.

ABSTRACT

Thríhnúkagígur Volcano, Iceland, is a composite spatter cone and lava field characteristic of basaltic fissure eruptions. Lava drainback at the end of the eruption left ~60 m of evacuated conduit, and a 4×10^4 m^3 cave formed by the erosion of unconsolidated tephra by the feeder dike. Field relationships within the shallow plumbing system provide three-dimensional insight into conduit formation in fissure systems. Petrographic estimates and the relative volumes of the cave and erupted lavas both indicate xenolithic tephra comprises 5–10 % of the erupted volume, which cannot be reproduced by geochemical mixing models. Although crustal xenolith entrainment is not geochemically significant, we posit that this process may be common in the Icelandic crust. The Thríhnúkagígur eruption illustrates how pervasive, poorly consolidated tephra or hyaloclastite can act as a mechanically weak pre-existing structure that provides a preferential pathway for magma ascent and may influence vent location.

KEYWORDS: Fissure; Eruption; Conduit formation; Volcanic vent; Crustal xenoliths; Reykjanes peninsula.

1 INTRODUCTION

Conduit development during basaltic fissure eruptions is an important process as it focuses magmatic flow leading to the development of eruptive vents (e.g. spatter and cinder cones, and tuff rings) and associated hazards. A synthesis of observations from both well-monitored and observed fissure eruptions [Sigmundsson et al. 2015; Gudmundsson et al. 2016; Pedersen et al. 2017; Gansecki et al. 2019; Neal et al. 2019] and exposed continental basaltic volcanic fields offers a model for conduit development during eruption [Delaney and Pollard 1981; Németh and White 2003; Keating et al. 2008; Genareau et al. 2010; Valentine 2012; Harp and Valentine 2015]. More deeply eroded fields reveal how magma is transported and stored in the shallowest levels of the crust immediately prior to and during eruption [Valentine and Krogh 2006; Kiyosugi et al. 2012; Richardson et al. 2015; Muirhead et al. 2016] and provide insights into how country rock properties and pre-existing structures affect magma propagation to the surface [Díez et al. 2009; Hintz and Valentine 2012]. Cooling and increases in magma viscosity in the feeder dike, and/or thermal and physical erosion of the country rock can lead to coalescence of flow from along the length of the fissure to isolated vents [Bruce and Huppert 1989; Wylie et al. 1999]. Eruptive activity and associated hazards are then focused at these vents. Basaltic volcanism is a global phenomenon found at all tectonic plate boundary types and in intracontinental settings [Wilson and Head 1981]. Therefore, new observations of conduits could lead to improved understanding of the processes leading to their formation.

1.1 Magma-country rock interactions

As magma migrates to the surface, thermal and/or physical erosion of the country rock contaminates the magma in the feeder dike through entrainment of xenoliths. This process can be facilitated by fracturing of the host rock in contact with the dike caused by increased pore pressure or shear stress imposed by the dike [Delaney and Pollard 1981; Macedonio et al. 1994; Brown et al. 2007; Townsend et al. 2015; Townsend 2018]. Eroded cinder cones provide evidence for the incorporation of crustal material where dikes flare open as they transition to more cylindrical conduits in the upper tens of meters of the crust [Wilson and Head 1981; Mastin and Ghiorso 2000; Mitchell 2005]. While these processes are important for conduit development and crustal xenoliths can provide information about the depths and geometry of the uppermost plumbing structure in these systems [Valentine and Groves 1996; Valentine 2012], crustal xenoliths are a volumetrically negligible proportion (commonly ≪1 %) of erupted material in lavas fed from basaltic fissure eruptions [Valentine and Groves 1996; Valentine 2012].

These same processes can also facilitate syn-eruptive emplacement of shallow intrusions. For instance, in the deeply eroded San Rafael Swell in Utah, saucer-shaped sills repeatedly intruded at depths of less than a kilometer [Pederson et al. 2002; Díez et al. 2009; Kiyosugi et al. 2012]. These sills are tens of meters thick and have volumes within an order of magnitude of the volume of eruptive products (10^{-4} to 10^{-1} km^3) at other small volume basaltic volcanoes [Richardson et al. 2015]. Similar intrusions at Paiute Ridge in Nevada also show how these intrusions can be controlled and affected by pre-existing structures in the crust such as faults and mechanically layered units [Valentine and Krogh 2006]. Other systems in the Amer-

*✉ michael.hudak@whoi.edu
✉ mike.r.hudak@gmail.com

ican Southwest show ductile deformation of the country rock in contact with intruded magma, and even magma diapirs as heat transfer and pore pressure increase lead to fluidization of the country rock [Díez et al. 2009; Hintz and Valentine 2012].

In contrast to these shallow magma-country rock interactions which primarily facilitate rapid mechanical incorporation of crustal material during magma transport, crustal assimilation occurs during magma storage over longer timescales. In longer-lived magmatic systems with persistent crustal reservoirs in Iceland, assimilated crust may account for as much as 10–30 % of erupted volumes of basalt, such as in the Grímsvötn-Laki system [Bindeman et al. 2008; Brounce et al. 2012] and at Krafla [Nicholson et al. 1991; Hampton et al. 2021]. Low-density and mechanically weak lithologies are common within the Icelandic crust on multiple scales from individual cinder cones and tephra layers to hyaloclastite units, including on the Reykjanes Peninsula [Marks et al. 2010; 2015]. These rheological heterogeneities in the crust, depending on the depths at which ascending magmas intersect them, may be involved in conduit formation, syn-intrusive stalling and assimilation [Gudmundsson and Loetveit 2005]. This begs the question of whether geochemical tools can identify crustal contamination during thermal and mechanical erosion during conduit formation in small volume basaltic fissure eruptions.

1.2 Geologic setting

The Reykjanes Peninsula in Iceland is a transtensional plate boundary [Sturkell et al. 1994; Taylor et al. 1994; Clifton and Kattenhorn 2006] that connects the submarine Reykjanes Ridge to the southern tip of the Western Volcanic Zone. It is composed of four volcanic systems that are structurally and petrologically distinct, the Reykjanes, Krísuvík, Brennisteinsfjöll, and Hengill (Figure 1; Einarsson and Sæmundsson [1987]). These volcanic systems lack well-defined central volcanoes like the other neovolcanic zones in Iceland [Thordarson and Larsen 2007; Einarsson 2008], are characterized by extensive northeast-striking *en echelon* fissure swarms, which are formed by repeated diking, fissure eruptions, and faulting [Gee et al. 2000; Árnadóttir et al. 2006; Clifton and Kattenhorn 2006], and the centers of production roughly follow the plate boundary [Thordarson and Larsen 2007; Sæmundsson et al. 2010]. Volcanism in the Reykjanes Peninsula seems to occur with ~1000-year periodicity, where most of the volcanic systems erupt within a time span of 200–400 years judging from the limited available geologic history [Clifton and Kattenhorn 2006; Sæmundsson et al. 2010; 2020]. The Brennisteinsfjöll volcanic system, approximately 45 km long and 10 km wide with several subparallel fissures, is considered to be the most productive system during the Holocene [Sæmundsson et al. 2020].

Thríhnúkagígur is a basaltic composite spatter cone located in the northern part of the Brennisteinsfjöll fissure swarm (Figure 2A). Thríhnúkagígur formed during a fissure eruption ~3.5 ka and is unique in that the upper eruptive conduit remained open due to lava drain back at the end of eruption (Figure 2B–C). The open conduit and a deeper cave allow direct observation of the three-dimensional structure of the magmatic plumbing system beneath the vent, including the
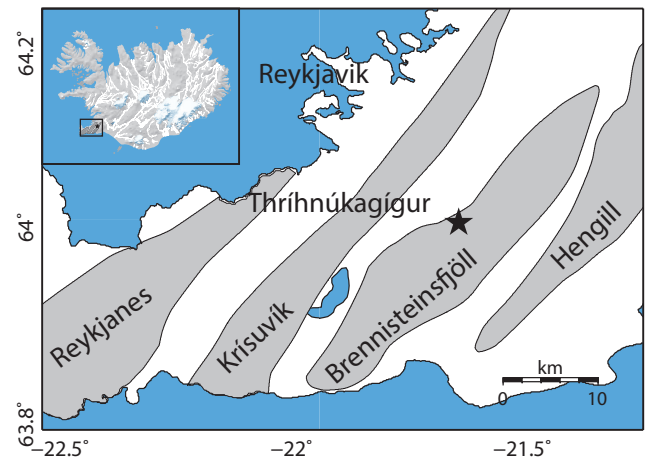

Figure 1: Map of the approximate boundaries of the four main volcanic systems of the Reykjanes Peninsula and the location of Thríhnúkagígur in the Brennisteinsfjöll system [Einarsson and Sæmundsson 1987]. The map corresponds to the box in the inset map of Iceland.

eruptive conduit and the feeder dike, and its association with the country rock. In the subsurface ~120 m beneath Thríhnúkagígur, there is a cinder cone-like unit consisting of partially palagonitized, unconsolidated basaltic glass ranging from fine ash to lapilli in size (which we refer to as tephra) buried under interglacial lava flows [Sæmundsson 2006]. We use field relationships, petrographic observations, and whole rock geochemical data to evaluate the role of tephra entrainment by ascending magma in the dike during eruption. These data allow us to draw inferences regarding the role of intruded country rock and its thermal and physical erosion on basaltic fissure eruption dynamics. Specifically, the analysis of the Thríhnúkagígur system will provide insights to how conduits form and evolve to focus magma flow at a vent, and how heterogeneity in the shallow crust impacts these processes and the ultimate locations of vents.

2 Field Descriptions

2.1 Surface geology

Thríhnúkar (Þríhnúkar) is a cluster of three peaks, Vesturhnúkur, Miðhnúkur, and Thríhnúkagígur, with each representing a constructional vent of a separate eruption (Figure 3A; Sæmundsson [2006]). Vesturhnúkur, the oldest and westernmost of the peaks, sits on the edge of a plateau that descends steeply to the northwest. It is a basaltic hyaloclastite unit associated with the late Weichselian glaciation [Sæmundsson et al. 2010]. Thin (cm to dm) dikes are pervasive on the western slope of the hyaloclastite and three dolerite plugs occur at the summit, likely representing eruptive conduits or vents that were subsequently eroded from the surface. It is older than the two subaerial Holocene eruptions, Miðhnúkur and Thríhnúkagígur. Miðhnúkur is a basaltic spatter cone between Vesturhnúkur and Thríhnúkagígur. It formed prior to Thríhnúkagígur and is estimated to have formed at ~5 ka, but its age is otherwise poorly constrained [Sæmundsson 2006].

Figure 2: The main edifice of Thríhnúkagígur is composed of two vents [A] and its southern vent remains evacuated and open, which is exploited to lower tourists into the conduit and cave system by a cable lift seen in yellow. Lava drainback textures are visible descending into the vent at the surface [B], which was a repeated and episodic process as is evident from the layers of thin clastogenic flows around the summit of the cone [C].

Lava flows from Miðhnúkur (Figure 3A) are the most extensive of the three Thríhnúkar eruptions with some outcrops up to 6.5 km away from the main cone and may extend further beneath subsequent lava flows [Sæmundsson et al. 2010]. One Miðhnúkur lava sample was collected in the lava field ~500 m northeast from its eruptive vent (Figure 3A). Locations and descriptions for all samples are provided for all samples in Table 1. The main edifice of Thríhnúkagígur, a 1.5 km long fissure and eruptive center [Sæmundsson 2006], formed from coalescence of two vents (Figure 2A). Soil profiles overlying Thríhnúkagígur lavas, which include >2.5 ka tephras from the Katla volcano, provide a minimum age and the eruption is estimated to be ~3.5 ka [Sæmundsson 2006; 2008]. Rising ~30 m above its surroundings, the cone is elongate along the azimuth of the fissure (Figure 3A). The northern of the two vents is sealed, while the southern vent remained open due to flow back of lava at the end of the eruption. The near vent facies are dominated by 2–10 cm thick, clastogenic flows that flowed down the upper flank and drained back into the vent and conduit (Figure 2C), similar to those discussed in Jones et al. [2018]. Smaller spatter cones within a couple hundreds of meters of Thríhnúkagígur to the south-southwest and another more than 1 km away to the north-northeast fed a total of three small lava flows (~0.1 km^2) in addition to the main

flow from Thríhnúkagígur, which covers 0.34 km^2 (Figure 3A; Sæmundsson [2006]). A perched lava pond, a common feature of fissure eruptions [Stovall et al. 2009; Pedersen et al. 2017], accumulated to the west and southwest of Thríhnúkagígur (Figure 3A) before draining to feed the lava field to the east a maximum lateral extent of 0.75 km from the vent.

Five samples of eruptive products were collected at Thríhnúkagígur (Figure 3A; Table 1). Two samples (TNG-33 and TNG-34) were collected from its lava field. One sample (TNG-37) was collected from a terrace or 'bathtub ring' of the lava pond. One sample (TNG-32) was collected from a several-meter-long lava lobe associated with a late-stage vent at the southern base of the main eruptive vent. The final sample (MC-612-03) is a large scoria clast collected at the summit of the spatter cone.

2.2 Subsurface geology

The southern vent of the Thríhnúkagígur eruptive center remains open providing access to both the evacuated conduit and to the cave below (Figures 3 and 4). A LiDAR survey of the conduit and cave system allows for detailed observations of the geometry of this system [LaFemina and Normandeau 2016; Zhao et al. 2019]. The conduit is elongated in the strike direction (north-northeast) of the eruptive dike and extends
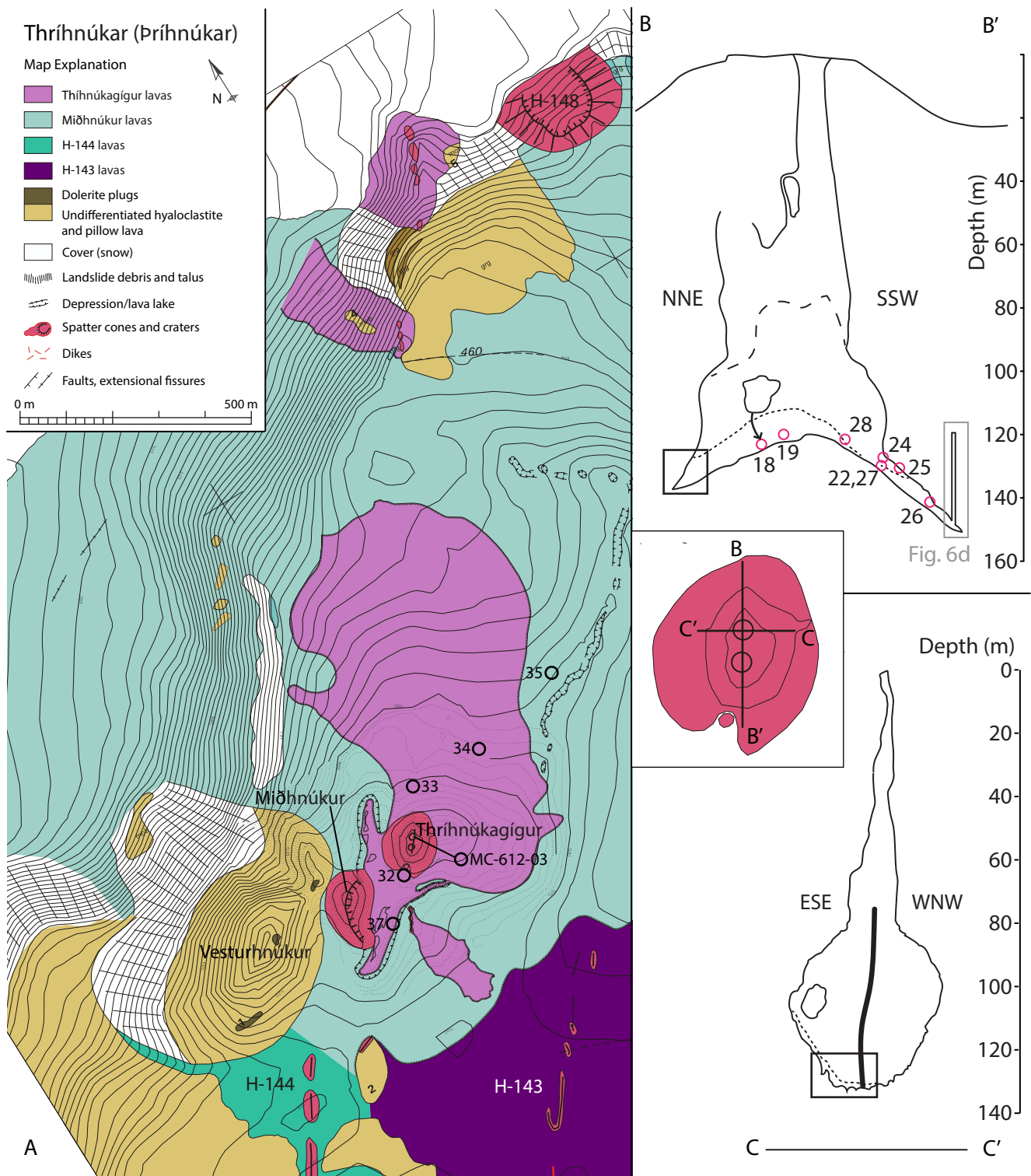
Figure 3: Map of the Thríhnúkar fissure system [A] modified from Sæmundsson [2006]. Erupted sample locations are shown in black circles. An enlarged inset of Thríhnúkagígur spatter cone shows the location of cross-sectional profiles of the cave below traced from LiDAR scans [LaFemina and Normandeau 2016; Zhao et al. 2019] both within the plane of the dike [B] and perpendicular to the dike [C]. Intrusive samples and samples of the tephra are shown with pink circles. The dotted line [B] represents the contact with the tephra. The dashed line [B] represents the roof of the cave and the uppermost extent of rock fall where the cave transitions into the narrower original conduit [C]. The small vertical pipe represents a proto-conduit (see Figure 6C, D). The boxes are illustrated in greater detail in Figure 4 with additional dike and buried tephra with sample locations.

Table 1: Thríhnúkagígur samples are subdivided into three groups: the erupted lavas, the intrusive components (dikes and the western wall intrusion), and tephra; along with a Miðhnúkur lava sample.

Sample ID	Sample Type	Description	Location/Latitude	Longitude
TNG-14-32	Lava	Flank vent flow	63.99775	−21.70025
TNG-14-33	Lava	Main vent flow	63.9993	−21.698
TNG-14-34	Lava	Main vent flow	63.99953	−21.6943
TNG-14-37	Lava	Main vent flow	63.99727	−21.70163
MC-612-03	Vent spatter	Main vent scoria	top of main vent	top of main vent
TNG-14-14m	Dike	Dike interior	Cave, NNE end	Cave, NNE end
TNG-14-24	Dike	Dike interior	Cave, SSW end	Cave, SSW end
TNG-14-25	Dike	Dike interior	Cave, SSW end	Cave, SSW end
TNG-14-27e	Dike	Chilled margin	Cave, SSW end	Cave, SSW end
TNG-14-27i	Dike	Dike interior	Cave, SSW end	Cave, SSW end
TNG-14-18	W Intrusion	Rockfall	Cave, N end	Cave, N end
TNG-14-15	Tephra	Unconsolidated	Cave, N/NNE	Cave, N/NNE
TNG-14-17	Tephra	Bomb (<10 cm)	Cave, N end	Cave, N end
TNG-14-19	Tephra	Unconsolidated	Cave, NNW end	Cave, NNW end
TNG-14-22	Tephra	Unconsolidated	Cave, NW end	Cave, NW end
TNG-14-26	Tephra	Unconsolidated	Cave SW/SSW	Cave SW/SSW
TNG-14-28	Tephra	Palagonitized	Cave SW/WSW	Cave SW/WSW
TNG-14-35	Lava	Miðhnúkur	63.99968	−21.69092

vertically 60 m down from the summit. The opening has a maximum dimension of ~10 m at the surface. The conduit constricts to a minimum width of 7.4 m at ~22 m depth, approaching the pre-eruptive paleosurface. Then, moving down away from the paleosurface, it widens slowly from 9.7 m at 45 m depth to 24 m at 60 m depth where it abruptly opens to the more cavernous region of the cave, which is shaped like a lung. At this depth, the conduit bifurcates with a ~15 m wide conduit corresponding to the now plugged northern vent of the Thríhnúkagígur edifice (Figure 3B). The ~60 m narrow, pipe-like portion of the conduit exposes very little of the subsurface stratigraphy because it is coated by lava drainback. Drainback on the conduit walls is characterized by rivulet textures (Figure 2B and Figure 5A) and stalactites of lava (Figure 5B) that are tens of cm in scale. Where drainback is absent or broken off, older lava flows and a few oxidized paleosols are exposed [Sæmundsson 2006]. At 36 m depth in the conduit there is a narrow, continuous tunnel that diverts off and reconnects to the main conduit in the shape of a teacup handle (Figure 3B). Originally mapped by cavers [Stefánsson 1992], this structure demonstrates the complexity of the shallow magmatic plumbing. Where the conduit opens into the broader cave at 60 m depth and below, drainback features no longer coat the cave walls, which is indicative of post-eruptive rock falls that occurred after lava drainback concluded. The floor of the cave is at a depth of ~120 m directly beneath the conduit, and it consists of rockfall (blocks of lava country rock from the ceiling) that have progressively moved the location of the cave upward to shallower depths through time. The maximum accessible depth of the cave, ~150 m, is to the south-southwest along the plane of the dike. The cave is 52 m wide and 86 m long at its maximum extent, and the walls expose the feeder dike at the north-northeast and south-southwest ends of the

cave. The dike varies in thickness and continuity within the cave walls (Figure 4) but does not exceed ~2 m in width. A succession of pre-Thríhnúkagígur basaltic lava flows, generally not exceeding a meter in thickness, comprise most of the cave walls. Their surface has been altered to a distinctive mustard yellow color (Figure 4).

Beneath the succession of lava flows is a geological unit that has previously been interpreted as a laterally continuous, gently dipping layer of hyaloclastite that breaks the surface at Vesturhnúkur [Sæmundsson 2006]. The unit has a cone-like morphology and is exposed in the northwest and western walls of the cave as well as deeper sections to the south-southwest. However, the physical characteristics of the hyaloclastite at Vesturhnúkur and the material in the cave are fundamentally different (Figure 5C). The surface hyaloclastite is indurated and variably palagonitized, whereas the unit in the cave consists primarily of unconsolidated glassy ash and scoriaceous lapilli that are only locally or weakly palagonitized. For this reason, we refer to this material as 'tephra' while acknowledging a co-genetic link between Vesturhnúkur and the tephra may be possible. The tephra is largely homogeneous in character with some localized, small-scale heterogeneity (Figures 4 and 5D). Most samples come from the relatively homogeneous tephra (TNG-15, TNG-19, TNG-22, TNG-26) including one ~10 cm scoria clast (TNG-17). Where the tephra cone is exposed in the northern wall, it slopes downward toward the feeder dike and 'interfingers' with some of the overlying lava flows (Figure 4). This sequence represents the progressive burial of the tephra cone, as well as erosion of the cone onto subsequent lava flows. At the lowest exposure in the north-northeast wall, the tephra extends laterally, possibly representing a tephra sheet or apron. Scoria clasts exceeding 10 cm in diameter were not observed in the tephra cone, but rare
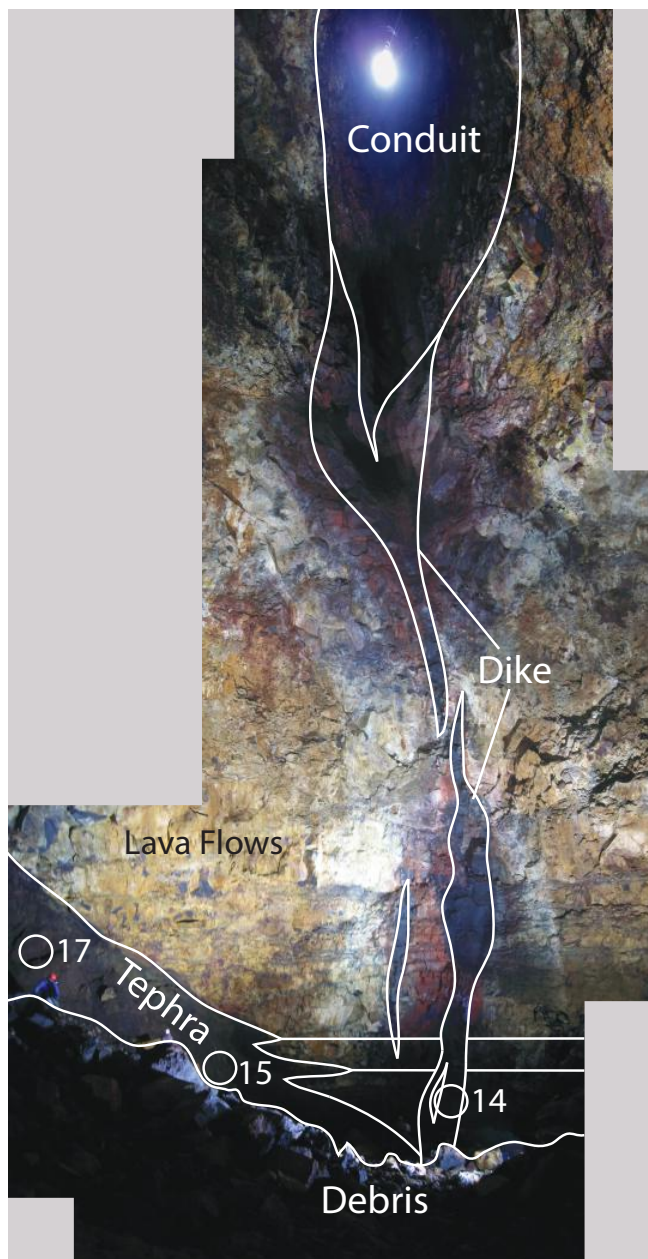
Figure 4: An annotated photo mosaic of the north-northeast cave wall photo mosaic shows the dike cutting through lavas from the base of the cave to the more cylindrical conduit and the surface vent. Additional sample locations are shown with white circles. The unannotated photo (Figure S1) can be found in the Data Repository [Hudak et al. 2022].

bombs and bomb sags occur in the tephra apron demonstrating the subaerial nature of this deposit. At the southwest end of the cave, an approximately 20 cm layer within the tephra is well consolidated with a quasi-foliated clay matrix around larger scoria clasts up to ~5 cm. One sample (TNG-28) was collected from this part of the deposit (Figure 3).

The feeder dike arcs continuously across the ceiling of the cave and down and through the north-northeast and south-southwest cave walls. Its north-northeast trend is consistent with the regional extensional fissures and crater rows of the

Brennisteinsfjöll fissure swarm. The dike is surrounded by a reddish contact aureole where it baked the intruded country rock. At the north-northeast end of the cave, the dike width and morphology changes with elevation. At the lowest exposure the dike is <50 cm wide and crosscuts the tephra. Just above this crosscutting relationship, the dike widens to nearly a meter (TNG-14m) and has an ~10 cm wide splay that separates and recombines with the wider dike. Although the dike is planar and continuous on the scale of the cave, it is locally discontinuous (in 2D). Two *en echelon* segments are observed about halfway up the north-northeast cave wall (Figure 4). Above the tephra cone in the northwestern wall of the cave, is ~5 m wide intrusion (Figure 5D; TNG-18). This intrusion is oval shaped with a large (gas) cavity in its center, is unaltered, and has a red, oxidized contact aureole, similar in appearance to the feeder dike. There is no visible surface manifestation of this intrusion, so it is interpreted to be a failed or abandoned conduit.

At the south-southwest end of the cave, the morphology of the dike is more complex. The dike is more vesicular with few vesicles in the margins of the dike (e.g. TNG-27e) and a gradational increase to higher vesicle content in the dike interior (e.g. TNG-27i), including one particularly impressive ~0.5 m long, 5 cm wide gas pocket (Figure 6A). Two additional samples were collected from this region of the dike (TNG-24 and TNG-25). Deeper in the southwest end of the cave, where the dike intersects the tephra, it becomes locally more distributed (Figure 6B). The best exposures of the dike are where it borders vertical cylindrical pipes, or "proto-conduits", that extend up into the tephra. These proto-conduits range in diameter from 0.25 to 2 m are typically immediately adjacent to the dike or within the plane of the dike and have drainback features along their walls (Figure 6C–D). A uniquely large hollow, cylindrical structure previously mapped by cavers (Figure 6C; Stefánsson [1992] and Sæmundsson [2006]) and with terrestrial LiDAR [LaFemina and Normandeau 2016; Zhao et al. 2019] is found at the deepest accessible extent of the cave. It penetrates more than 30 m up into the overlying tephra and is mostly coated in drainback textures (Figure 6D).

3 METHODS

Samples collected for this study (locations in Figure 3A–C and Figure 4) were analyzed with petrographic and geochemical techniques to investigate the nature of Thríhnúkar intrusive and eruptive components, and the potential role of crustal entrainment in the formation of conduits during basaltic fissure eruptions.

3.1 Petrography and BSE imaging

The modal abundances of groundmass and crystalline phases were determined by point counting 200–400 gridded points using a petrographic microscope [Data Repository Table S1: Hudak et al. 2022]. Backscattered electron (BSE) images of tephra glasses and microxenolithic glass fragments in lavas were collected on a Cameca SX-5 electron microprobe (EPMA) in the Materials Characterization Laboratory at The Pennsylvania State University (Penn State). An accelerating voltage of 15 keV and a beam current of 30 nA were used with a de-
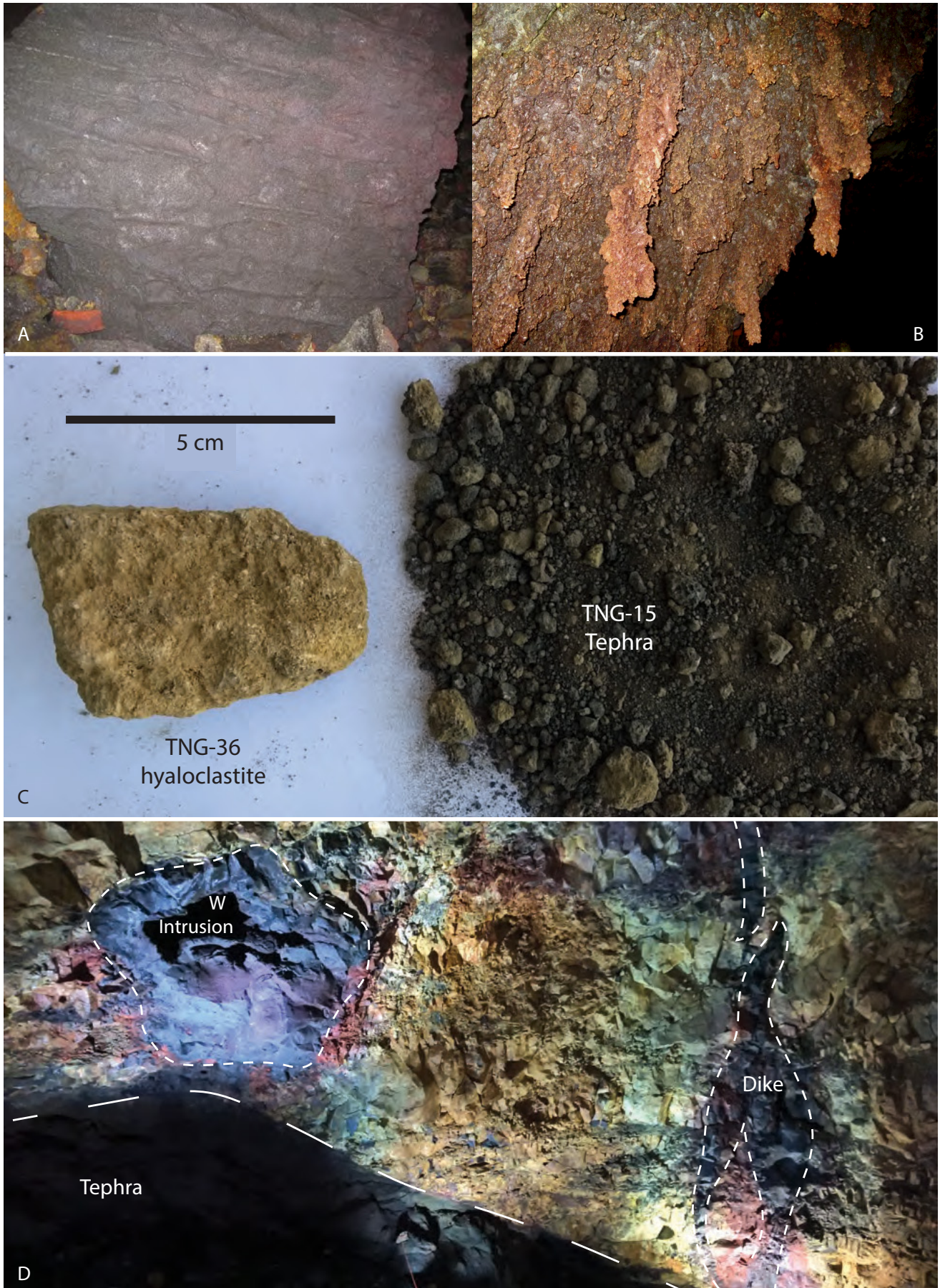
Figure 5: (Caption next page.)

Figure 5: (Previous page.) [A, B] Rivulets of lava drainback on a 1–2 m wide fallen block of the conduit wall [A] and lava stalactites [B] that are 0.2 to 0.4 m long. [C] The Vesturhnúkur hyaloclastite (left; TNG-36) is different in appearance from a characteristic sample of the tepha in the cave (right; TNG-15). Notably TNG-36 is well consolidated relative to TNG-15. [D] Photograph of field relationships in the cave showing the western wall intrusion directly above the tephra and the main feeder dike just above where it crosscuts the lowest exposure of tephra in the NNE end of the cave. .
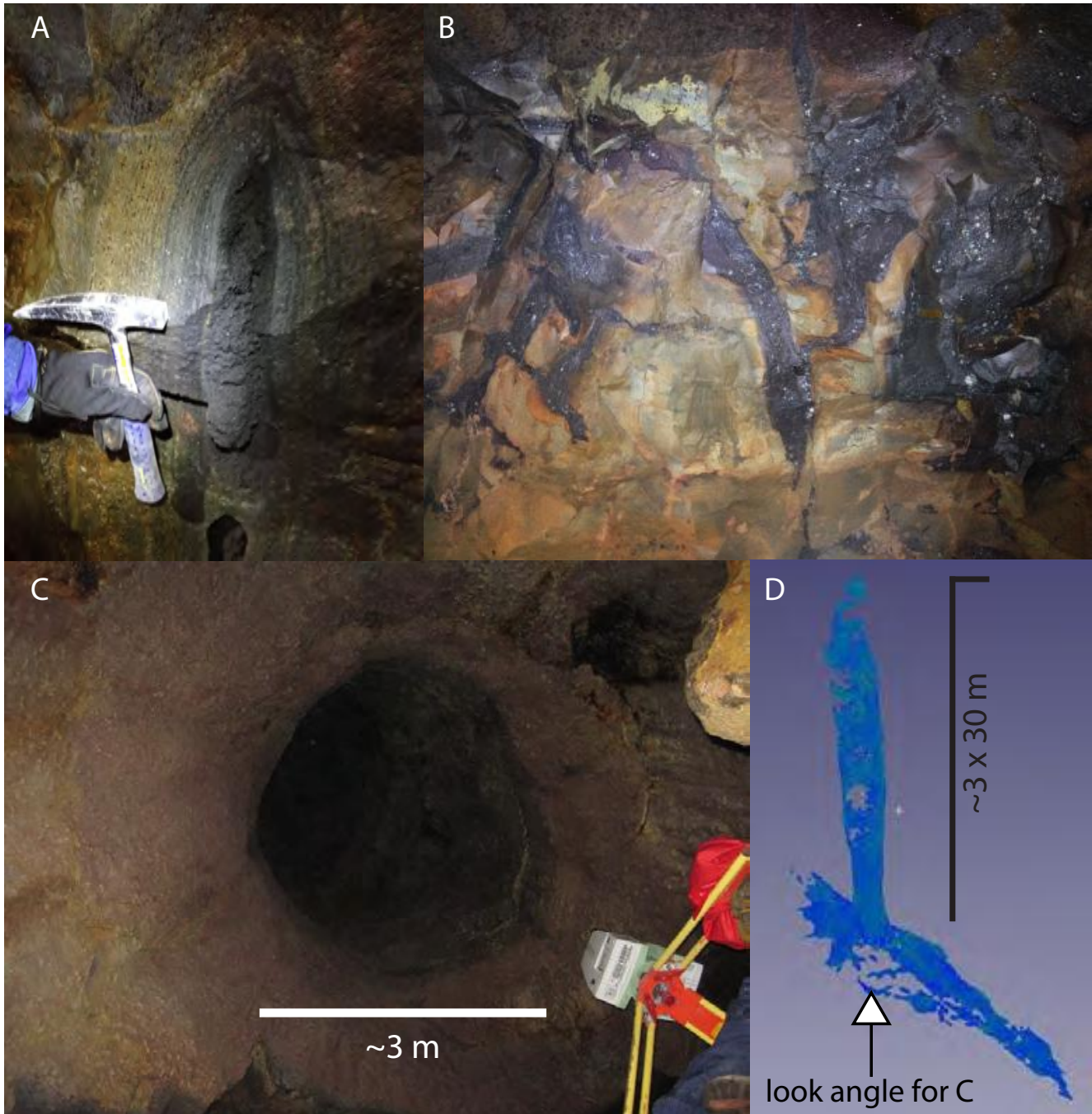
Figure 6: [A] A large vesicle captures annular gas flow through the conduit system. [B] Small irregular intrusions several cm wide and ~20 cm long infiltrate a rare, well consolidated (possibly by alteration) section of tephra in the cave, illustrating how less well consolidated tephra was likely to have been intruded and incorporated into the ascending magma. This exposure occurs in the center of the main dike in the narrow crawl space descending into the deepest part of the south end of the cave (Figure 3B) near where a 3-meter-wide cylindrical conduit [C] is exposed. LiDAR images [D] show that it extends vertically 30 meters upward within the plane of the main feeder dike.

focused 10 µm beam. The produced X-ray intensities were subject to a PAP (phi-rho-z) matrix correction algorithm and converted to concentrations by comparison to natural and synthetic standards.

3.2 Bulk rock geochemistry

Bulk rock major and trace element concentrations were determined at the Laboratory for Isotopes and Metals in the Environment (LIME) at Penn State to evaluate geochemical heterogeneity and processes in the Thríhnúkar system. Splits of 100 mg sample powder were weighed and mixed with 1 g of lithium metaborate. The mixtures were transferred to graphite crucibles and heated to 1000 °C for 10 minutes. The resulting melts were added to 100 mL of 5 % HNO_3 solution for a total dilution factor of ~1000. These solutions were analyzed for major element concentrations using a Perkin-Elmer Optima 5300DV Inductively Coupled Plasma Atomic Emission Spectrometer (ICP-AES).

Trace element concentrations were analyzed on a Thermo X-Series II Quadrupole Inductively Coupled Plasma Mass Spectrometer (ICP-MS) following the methods of Kelley et al. [2003]. Calibration curves with R^2 ≥0.999 were made using a method blank and five reference materials: BHVO-1, BCR-1, BR, BIR-1, and JA-1[*]. The instrumental background was determined using a 2 % HNO_3 solution in milli-Q water. Backgrounds for each trace element were ≤0.01 ng g^{-1} for all elements except Ni, Sc, Cu, Cr, and Zn. Samples TNG-18 and TNG-27e were duplicated in two analytical sessions. For these replicate analyses, reported values for most analytes are repeatable within 5 %. The elements Sc, V, Co, Cu, Sr, Ce, Lu, and U were all within 8 %. Only Ta was higher with an 18 % difference at <0.5 mg g^{-1} in the rock.

Isotope ratio measurements of Sr and Nd were conducted at the Consiglio Nazionale delle Ricerche, Pisa, Italy on a Finnigan MAT 262 multi-collector thermal ionization mass spectrometer (TIMS) running in dynamic mode. Acid digestion, ion chromatography, and analytical procedures were conducted according to the methods in Cannaò et al. [2015]. Ratios of $^{87}Sr/^{86}Sr$ are normalized to $^{86}Sr/^{88}Sr$ of 0.1194 and the mean $^{143}Nd/^{144}Nd$ ratios are normalized to $^{146}Nd/^{144}Nd$ of 0.7219. The results of 19 analyses of Sr standard NIST SRM 987 (SrCO$_3$) gave an average of 0.710227 ± 0.000020 (2σ). Measured values are corrected to $^{87}Sr/^{86}Sr$ = 0.710250 for SRM 987, and this correction factor is applied to the unknowns. Blanks for Sr are <0.3 ng and are negligible. Twenty-seven analyses of the Nd standard JNdi-1 yield 0.512104 ± 0.000010 (2σ). No correction was made.

4 Results

4.1 Petrographic and textural descriptions

4.1.1 *Lavas*

Lava samples from Thríhnúkagígur (*n* = 4) are vesicular (18–36 % by volume) with a vesicle-corrected 15–20 % plagioclase phenocrysts [Data Repository Table S1: Hudak et al. 2022]. The modal abundance of plagioclase in the scoria clast from

---

[*]preferred values for reference materials available at https://georem.mpch-mainz.gwdg.de/ [Jochum et al. 2005].

the vent is slightly lower at 11 %. Plagioclase phenocrysts are primarily shorter than 3 mm in length, with rare phenocrysts up to 1 cm. Plagioclase glomerocrysts reach 1 cm in diameter. The groundmass consists of thin plagioclase laths ~100–200 µm in length, globular or dendritic oxides up to a few microns in length, and clinopyroxene not exceeding 10–20 µm. In contrast, the Miðhnúkur lava sample (TNG-35) contains 5–8 % olivine phenocrysts up to 1.5 mm in length. Macroscopic olivine glomerocrysts in hand sample up to 4–5 mm uniformly consists of euhedral, equant crystals that are each 1–1.5 mm in length. The groundmass consists of thin plagioclase laths up to ~100 microns in length, skeletal olivine crystals up to ~50 microns in length, and dendritic oxides up to a few microns in length. Lava samples TNG-33 and TNG-37 from Thríhnúkagígur and, notably, TNG-35 from Miðhnúkur contain vesicles up to ~1–2 mm in diameter that are filled or partially filled with fragments of glass and palagonite (Figure 7). The groundmass surrounding the infilled vesicles is commonly oxidized. The fragments inside the vesicles vary from micron-sized particles up to as large as 200 microns and are typically on the order of tens of microns in diameter. The glassy fragments are typically angular, dense, and free of microlites, although scoriaceous fragments and rare plagioclase microlites are observed. Some glassy fragments have palagonite rims. The palagonite fragments are friable, heterogeneous, and angular to sub-rounded. While these clusters of glass shards most commonly occur in vesicles, they are also present integrated into the groundmass (Figure 8).

4.1.2 *Dikes*

Dike rocks are texturally heterogenous. The margins of the feeder dike are quenched in places, with a fine-grained groundmass and few phenocrysts on the dike margins. In one dike sample from the SSW end of the cave (TNG-27), the contact between the outer quenched margin and interior of the dike is sharp. In other places, the transition from the quenched margin to the dike interior is more gradational. The interface between the quenched margin and the dike interior, where present, is often marked by a line of mm-scale vesicles with bubble walls that are commonly oxidized. The interior of the dike has a more coarse-grained groundmass, plagioclase laths that are generally aligned parallel to the flow direction, and interstitial clinopyroxene phenocrysts. Vesicles are observed in both the interior and quenched margin of the dike but are more common in the interior. A large gas pocket "froze" in the center of the main dike, capturing the annular flow consistent with Hawaiian to Strombolian style eruptions (Figure 6A; Houghton et al. [2021]).

4.1.3 *Tephras*

The tephra from within the cave consists primarily of scoriaceous clasts ranging in size from a fine ash (<125 µm) to 2–3 cm lapilli (Figure 5C). The tephra clasts contain abundant plagioclase microlites (Figure 9A–C) and are variably devitrified or palagonitized. Some clasts also contain 1–2 % globular or dendritic oxides on the order of a few microns in length, texturally similar to those observed in the groundmass of erupted lavas. Macroscopically, clasts containing oxides appear black while those without appear brown. Loose
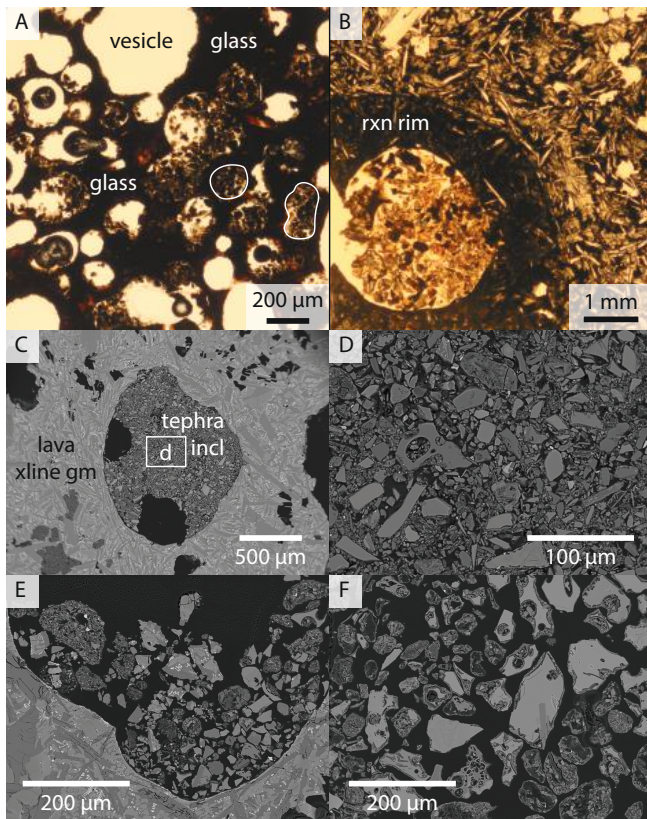
Figure 7: Plane polarize light images of Thríhnúkagígur vent spatter, MC-612-03 [A], and lava, TNG-33 [B] and BSE images of lavas [C–F] show how vesicles are filled with annealed glass shards. ([C–D]: TNG-33; [E]: TNG-35; [F]: TNG-37). The TNG-35 lava sample from Miðhnúkur suggests that entrainment of near surface unconsolidated tephra has occurred multiple times at the Thríhnúkar system through time.
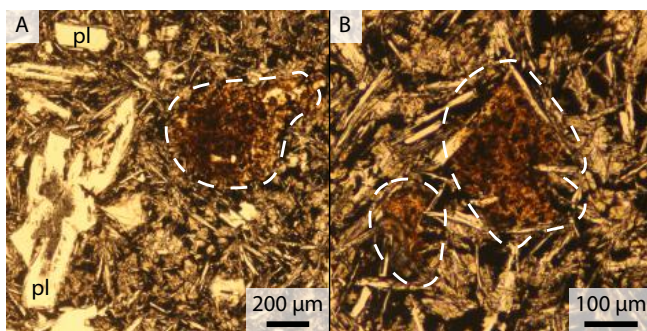

Figure 8: Plane polarized light images show entrained tephra incorporated as a coherent and well-integrated mass into the groundmass of lava sample TNG-33.

plagioclase and olivine crystals are present but uncommon (Figure 9A–B). Variably vesicular, angular, glassy ash particles comprise both the tephra (Figure 9C; TNG-19) and a hyaloclastite intersected at the surface by the Thríhnúkagígur feeder dike (Figure 9D; TNG-29, not analyzed for geochemistry). In general, the ash particles in the tephra contain a greater density of plagioclase microlites and a lower extent of palagonitization than the hyaloclastite.
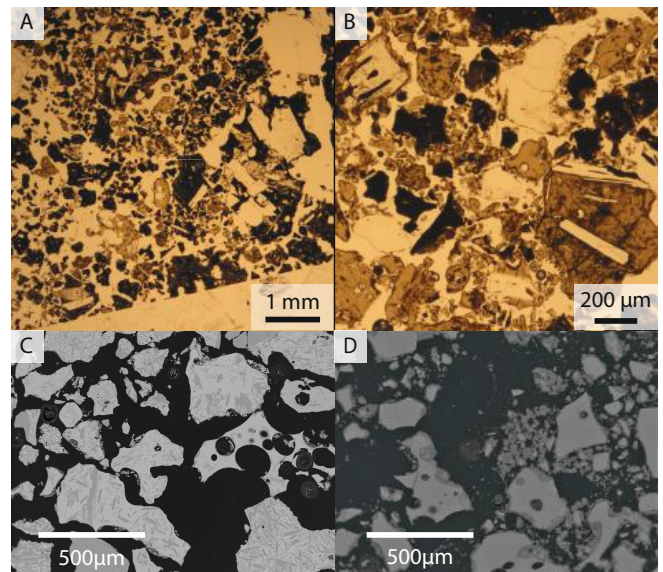
Figure 9: Plane polarized images of tephra samples TNG-19 [A] and TNG-22 [B] and BSE images of TNG-19 [C] and a BSE image of hyaloclastite, TNG-29 [D]. Tephra and hyaloclastite alike primarily consist of glass fragments with some loose crystals and larger, commonly phenocryst-bearing lapilli.

4.2 Geochemical data

Lava and dike samples from the Thríhnúkagígur eruption and the tephras exposed at depth within the cave are all basaltic and span a range of 6.03–9.58 wt.% MgO [Figure 10; Data Repository Table S2: Hudak et al. 2022]. This range is consistent with tholeiitic Holocene lavas of the Reykjanes Peninsula [Jakobsson et al. 1978; Gee et al. 1998; Kokfelt 2006; Peate et al. 2009; Koornneef et al. 2012]. However, Thríhnúkagígur volcanics fall at the low end of the range for SiO_2 and MgO compositions for Reykjanes lavas and at the high end for Al_2O_3. The lavas are the most homogeneous group of samples (47.7–48.2 wt.% SiO_2; 12.20–13.04 wt.% Fe_2O_3; 7.21–7.74 wt.% MgO; 11.89–12.01 wt.% CaO). In contrast, dike samples are rather more heterogeneous (47.23–49.25 wt.% SiO_2; 10.78–13.20 wt.% Fe_2O_3; 7.54–9.58 wt.% MgO; 11.84–13.38 wt.% CaO). One sample (TNG-18), collected from the talus pile in the cave directly beneath the western wall intrusion and proposed to be from the intrusion, has the most primitive (MgO-rich, SiO_2-poor) major element composition, which cannot be explained simply by plagioclase removal from the dike samples. Similarly, a margin of the dike (TNG-27e) has the highest SiO_2 and CaO and the lowest TiO_2, K_2O, Na_2O, and Fe_2O_3 of any sample from the Thríhnúkagígur eruption (Figure 10). The tephra exposed within the cave is distinct from the products of the Thríhnúkagígur eruption with more evolved composition (46.70–48.38 wt.% SiO_2; 13.45–14.09 wt.% Fe_2O_3; 6.03-6.76 wt.% MgO; 9.79–11.50 wt.% CaO) and loss on ignition (LOI) values of 0.69–2.79 wt.%, suggesting variable alteration, weathering, or glass rehydration. The tephra is more enriched in TiO_2, K_2O, and P_2O_5 than Reykjanes lavas (Figure 10).
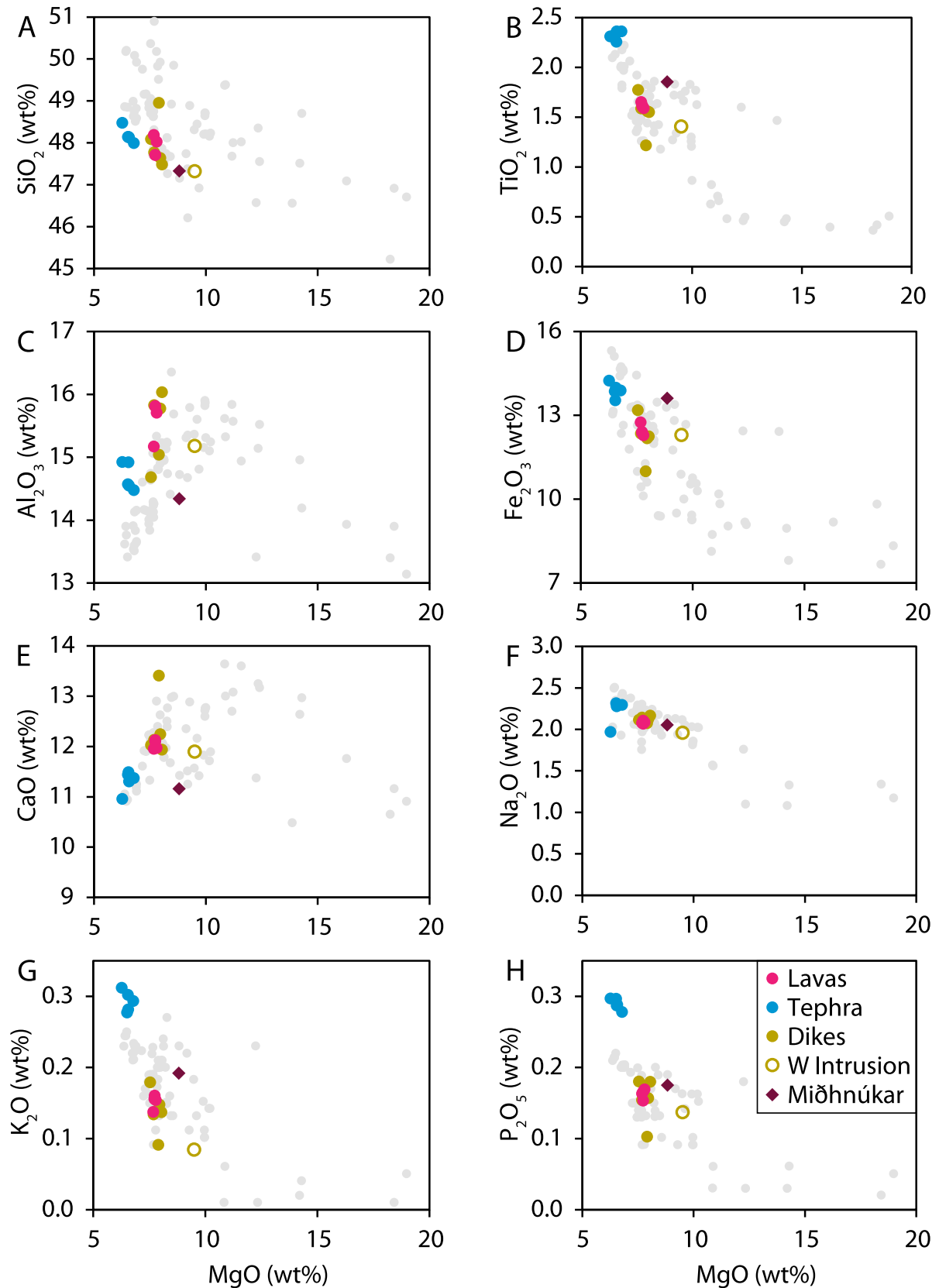
Figure 10: (Previous page.) Major element plots of MgO vs. SiO_2 [A], TiO_2 [B], Al_2O_3 [C], Fe_2O_3 [D], CaO [E], Na_2O [F], K_2O [G], and P_2O_5 [G] for Thríhnúkagígur lavas, the tephra exposed in the cave, the dikes, the western wall intrusion, and Miðhnúkur. Gray circles are published data for lavas on the Reykjanes Peninsula [Jakobsson et al. 1978; Gee et al. 1998; Kokfelt 2006; Peate et al. 2009; Koornneef et al. 2012].
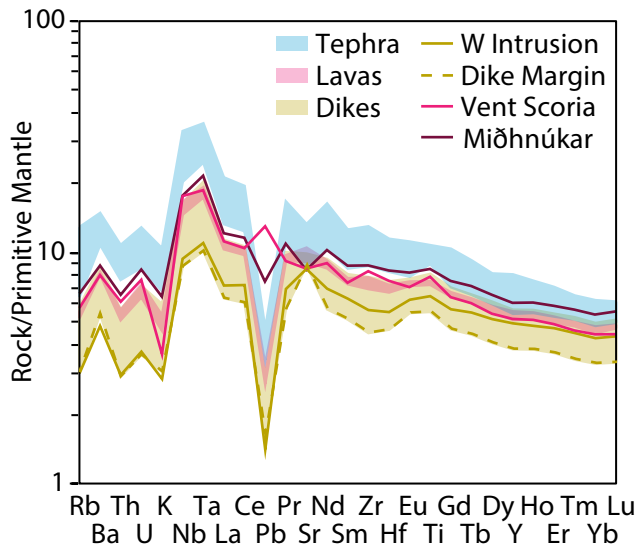
Figure 11: Primitive mantle normalized multielement diagram for Thríhnúkagígur samples show that the tephra are uniformly enriched in incompatible trace element relative to the lavas or dikes and that the lavas are homogeneous relative to their corresponding intrusive rocks. Primitive mantle normalization values are from [Sun and McDonough 1989].

A primitive mantle normalized multi-element diagram [Sun and McDonough 1989] also demonstrates how the intrusive components (the western wall intrusion and the dikes) of the system have a greater range in incompatible trace element concentrations than in the corresponding erupted lavas (Figure 11). All samples in these multi-element diagrams are characterized by strong positive Nb and Ta anomalies, positive Ba and U anomalies, and large negative Pb anomalies (except the vent scoria, MC-612-03, which has a small positive Pb anomaly most probably a sign of contamination related to construction of the tourist elevator at the vent; Figure 11; [Data Repository Table S2: Hudak et al. 2022]). Strontium displays a negative anomaly in the tephra, a positive anomaly in the chilled dike margin (TNG-27e) and western wall intrusion (TNG-18), and lacks noteworthy anomalies in the majority of dike and lava samples. In general, the tephras have higher concentrations of incompatible trace elements than the lavas and dikes and have roughly parallel profiles (Figure 11).

Thríhnúkagígur volcanics have Sr-Nd isotope compositions consistent with the published range of values for the adjacent volcanic system, Krísuvík, but greatly expanding the range of $^{87}Sr/^{86}Sr$ ratios for Brennisteinsfjöll (Figure 12). The lavas and dikes span nearly the same range of Sr-Nd isotope ratios as the tephra. Three dike samples define the lowest $^{87}Sr/^{86}Sr$ values (0.70313 to 0.70314, Figure 12; [Data Repository Table S2: Hudak et al. 2022]). A tephra (TNG-22) has the most radiogenic $^{87}Sr/^{86}Sr$ ratio of 0.70330, followed by a lava sample (TNG-34) with $^{87}Sr/^{86}Sr$ = 0.70328. Ratios of $^{143}Nd/^{144}Nd$ range from 0.51299 to 0.51305 (Figure 12). Despite the narrow range, the tephras are on average less radiogenic than the lavas and dike samples. With the exception of the most altered tephra sample (TNG-28; LOI = 2.79 wt.%), the Nd

isotopic values of the tephras do not exceed 0.51302. A single lava sample (TNG-32) has a $^{143}Nd/^{144}Nd$ ratio within the range of the tephra, while all other dike and lava samples have ratios ≥0.51302.

5 Discussion

Direct observations of the shallow magmatic plumbing systems of basaltic fissures along with associated and intact eruptive vents are rare [Lefebvre et al. 2012; Geshi and Neri 2014; Hughes et al. 2018]. Thríhnúkagígur presents an opportunity to not only view both the intrusive structures at shallow depth and extrusive components of a small-volume basaltic fissure eruption but allows the investigation of the link between intruded magmas, country rock (i.e. the buried tephra) and eruptive products. In the following we discuss our petrologic, geochemical, and geologic observations of this system, which shed light on the relationship between crustal entrainment and conduit formation along a basaltic fissure, and the geometric complexity of shallow feeder dike systems.

5.1 Conduit development and syn-eruptive cave formation by tephra entrainment

The formation of conduits and the construction of eruptive centers during basaltic fissure eruptions focuses magma flow, potentially changing the hazards and risks of the eruptive phenomena. Commonly, eruption initiation occurs along segmented *en echelon* dikes that form due to rotation of the local minimum stress direction as the dike approaches the surface [Pollard et al. 1975; Delaney and Pollard 1981; Rubin 1995; Roman and Cashman 2006]. Subsequent focusing of magma flow from an eruptive fissure to an approximately cylindrical point source feeding eruptive vents is facilitated by cooling along and within a dike and increases in magma viscosity, as well as by thermal and physical erosion during basaltic fissure eruptions [Bruce and Huppert 1989; Wylie et al. 1999]. However, the comparative role of these processes in conduit formation and vent focusing is seldom clear during an eruption. The surficial geology of the Thríhnúkagígur eruptive system does not indicate that eruptive dynamics here were demonstrably different than other basaltic fissure eruptions, despite the anomalous physical erosion in the conduit. It has all the common hallmarks of basaltic fissure eruptions, several briefly active vents and a main spatter cone that fed a small lava field [e.g. Keating et al. 2008; Valentine and Gregg 2008; Németh and Kereszturi 2015]. Other structures are similarly commonplace, such as the perched lava pond that later drained [Stovall et al. 2009; Patrick and Orr 2012] and clastogenic flows back into the main vent [Parcheta et al. 2012; Jones et al. 2017; 2018]. Yet, the upper conduit of the main eruptive center remained open at the end of the eruption and there is a deeper cave that make this system remarkable. While caves are also common in basaltic fissure systems as lava tubes, these extend laterally away from the vent and feed the growing lava field [Peterson et al. 1994; Orr et al. 2015; Gudmundsson et al. 2016] rather than extending vertically down from the vent. However, given how common lava drainback is in these systems [Richter et al. 1970; Swanson et al. 1979; Patrick et al. 2015], evacuated segments of conduits should perhaps not be such an unex-
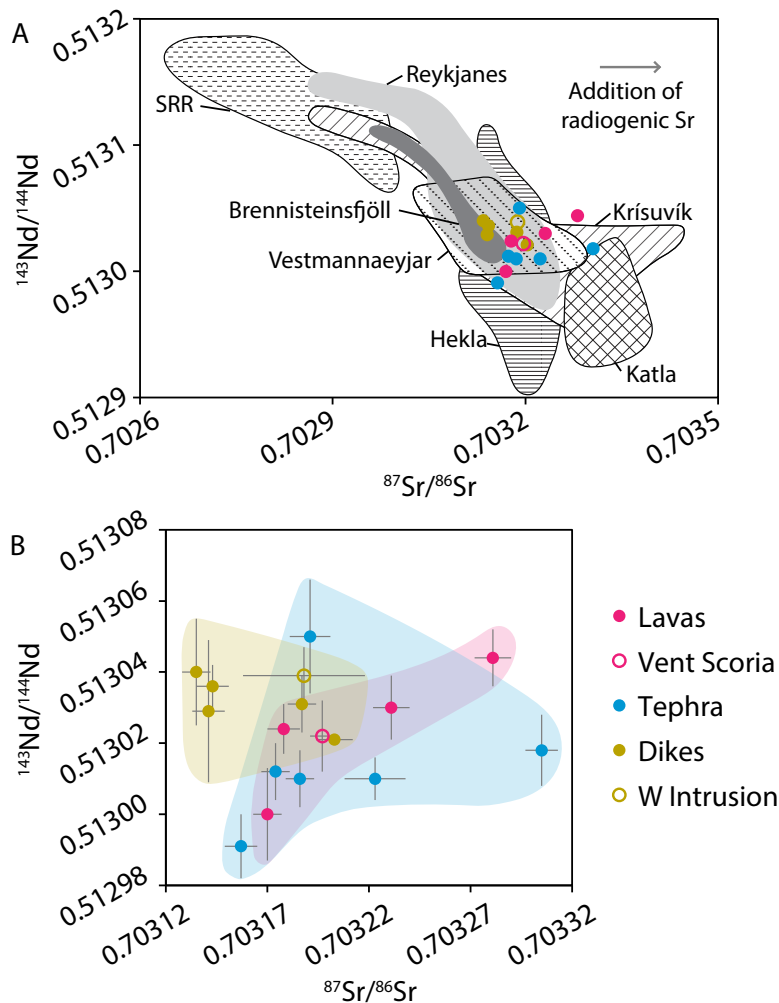
Figure 12: [A] Sr-Nd isotope ratios Thríhnúkagígur samples are compared to the Southern Reykjanes Ridge (SRR) and several volcanic systems in southern Iceland [Park 1990; Furman et al. 1991; Sigmarsson et al. 1992; Furman et al. 1995; Thirlwall et al. 2004; Kokfelt 2006; Peate et al. 2009]. They greatly expand the range of values for Brennisteinsfjöll and occupy the more enriched end of the observed Reykjanes Peninsula compositions. [B] All sample types at Thríhnúkagígur have in ^{87}Sr/^{86}Sr and ^{143}Nd/^{144}Nd ratios, although lavas (pink) are generally intermediate in compositions between the dikes and western wall intrusion (yellow) and the tephra (blue).

pected feature [Wadsworth et al. 2015]. Here, we exploit the exposed subsurface geology to investigate conduit and vent forming processes, and the role of crustal heterogeneities in focusing magmatic flow and conduit formation through physical erosion. There are clear spatial correlations between the feeder dike, the buried tephra deposits exposed in the cave (the country rock), and proto-conduits and the main eruptive conduit (Figure 6C–D). Furthermore, the presented petrographic observations indicate the presence of tephra in erupted lavas (Figures 8 and 9). To our knowledge, there is no exposed system that directly compares to the size and orientation of Thríhnúkagígur. We propose that magmatic scouring and incorporation of the unconsolidated tephra focused magma flow along the Thríhnúkagígur fissure forming the conduit and main eruptive center. Furthermore, the erosion of the buried tephra created a void, which then collapsed following the end of eruptive activity. We envision the Thríhnúkagígur system evolved during the eruption according to the following conceptual model (Figure 13). A subaerially erupted tephra cone, now buried at ~120 m depth beneath younger lava flows (Figure 13A), was intersected by the feeder dike at the onset of the fissure eruption that formed Thríhnúkagígur (Figure 13B). As the intrusive-eruptive event progressed, turbulent flow in the upper reaches of the dike [Valentine and Gregg 2008] and/or wall rock instability [Carey and Houghton 2010] was able to

physically erode and entrain the unconsolidated tephra (Figure 13C). We propose that the erosion of the tephra, likely 100–200 m below the surface, focused magma flow at this location along the dike leading to conduit formation and formation of the southern and northern eruptive vents (i.e. the Thríhnúkagígur cone) as opposed to other vents along the fissure. At the end of the eruption, magma was drained into the conduit and along the fissure at depth, which is preserved in drainback features (Figure 2C and Figure 5C–D). Both the 1959–60 eruption of Kīlauea Iki [Richter et al. 1970] and the 1969–71 eruption of Maunaulu [Swanson et al. 1979] had multiple episodes of lava drainback without the formation of new vents. Finally, the void left by the scoured tephra and lava drainback caused collapse of the overlying lava pile, formation of the lung-shaped cave, and the talus pile at the base of the cave, exposing the dikes and intrusive structures visible today (Figure 13D). This effectively moved the location of the cave upwards to shallower depths than where tephra entrainment was most extensive. While some downward transport of blocks of country rock within conduits has been observed in eroded systems [Richardson et al. 2015], Thríhnúkagígur cave evolution has clearly been dominated by post-eruptive rockfall in the intervening ~3.5 ka. The above conceptual model for focusing magma flow and formation of the conduit also
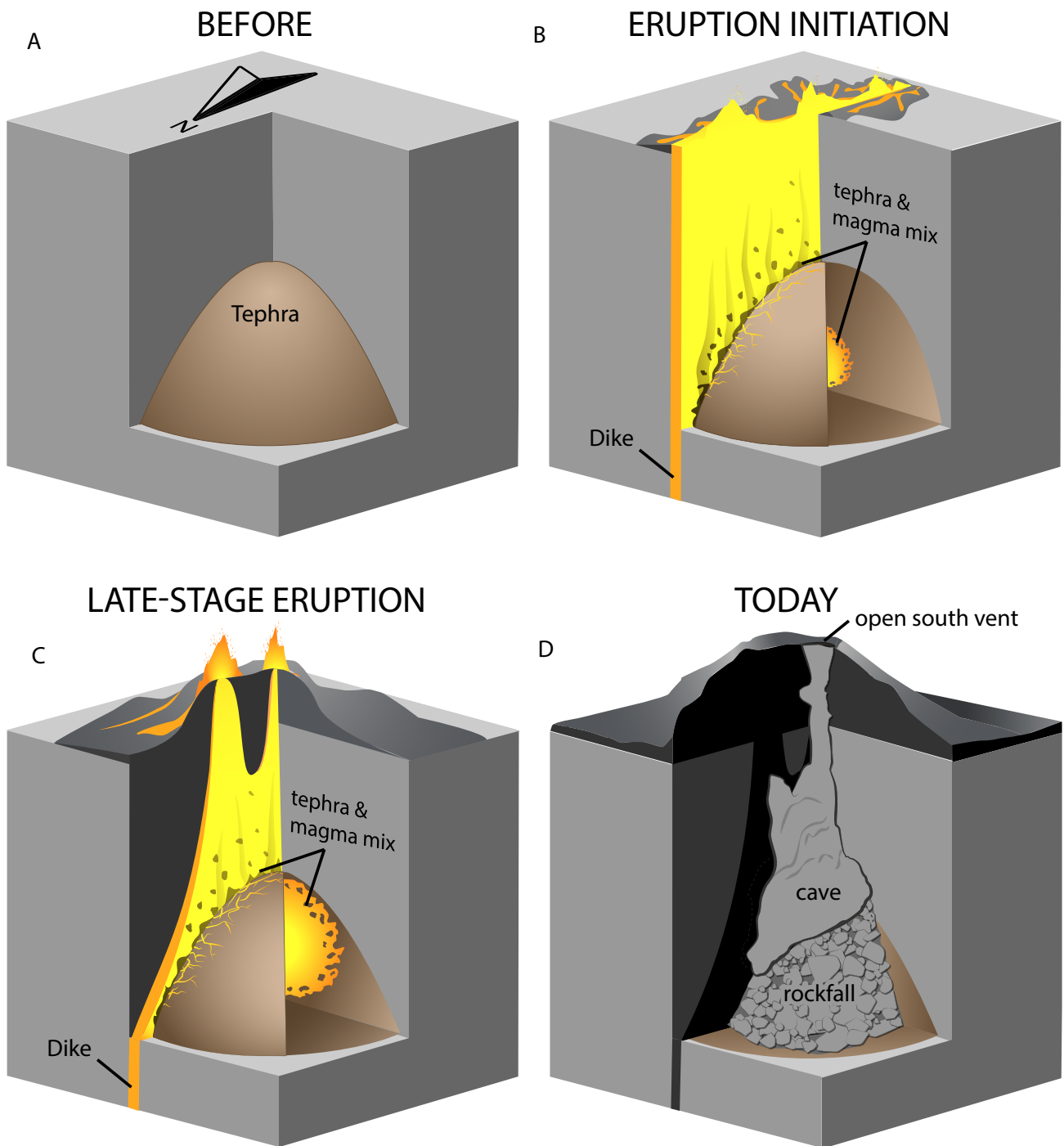
Figure 13: Block diagram of cave formation during the eruption of Thríhnúkagígur. Prior to eruption [A] a tephra cone is buried under lava flows. At the onset of eruption [B], a dike crosscut the tephra and overlying lavas, commencing a fissure eruption with multiple events and limited interaction with the intersected tephra body. As the eruption progressed [C], unconsolidated tephra was entrained by the dike and flow became focused at two vents. Tephra incorporation created vacancy beneath the vent, within the conduit. As the eruption ended, lava drainback left the south vent evacuated and open to the surface. Rockfall from the cave ceiling has filled much of the region where tephra had been incorporated and moved the cave upward from its original location in the conduit into overlying country rock [D]. Illustration by Natalie Renier, WHOI Creative Studio © Woods Hole Oceanographic Institution.

works for Miðhnúkur, as evidenced by the presence of tephra in sample TNG-35.

Evidence for magmatic scouring of the tephra deposit is three-fold. First, in the deepest extent of the cave, ~150 meters below the paleo-surface, the dike is locally dispersed with thin, centimeter- to decimeter-wide segments within the tephra deposit (Figure 6B). These structures show one mechanism by which ascending magma disaggregated and mechanically incorporated blocks of wall rock. This process eventually led to large-scale excavation and incorporation of shallow crustal material into the erupted lavas (Figure 13). Second, magmatic erosion of the tephra is strongly focused and best observed in the vertical, cylindrical proto-conduits ranging from 10s of cm up to 30 m in height that are etched into the tephra (Figure 6C–D). Finger-like intrusions in shallow conduit systems, like the proto-conduits at Thríhnúkagígur, are predicted in some numerical models [Whitehead and Helfrich 1991; Wylie and Lister 1995; Wylie et al. 1999; Gudmundsson and Loetveit 2005] and observed on small scales near the surface adjacent to monogenetic basaltic dikes [Hintz and Valentine 2012]. Shallow ductile deformation (<2 km) can also facilitate basaltic diapirism through porous, low-density crustal materials [Díez et al. 2009]. These observations clearly demonstrate how ascending magmas can take advantage of rheological or lithological heterogeneities in the upper crust to focus magma flow from a dike to a conduit over a vertical scale of a few meters. Finally, petrographic observations of surface flows from both Thríhnúkagígur and Miðhnúkur provide evidence for tephra incorporation into the magma. Lava samples contain clusters of tephra shards in a variety of textures. The tephra primarily consists of ash-sized glass shards (Figures 7 and 8), which appear in Thríhnúkagígur lavas in two forms: within vesicles and along vesicle walls (Figure 7) and incorporated as a constituent of the glassy groundmass matrix (Figure 8). Some tephra shards are homogenous glasses with several microns of palagonite rims, making it unlikely that the tephra are small fragments of melt related to fire fountaining. Clusters of tephra shards comprise 4–8 % by volume in the lava samples in thin sections. This is a minimum estimate as individual glass shards may become indistinguishable from the matrix glass, especially because the tephra has nearly identical physical and chemical properties to the magma.

Multiple methods can be used to estimate the mass contribution of tephra to the erupted lavas, including petrographic analysis or geochemical and isotopic mixing calculations, as presented in Section 5.3. It is important to note that each of these methods only gives a first order approximation of volume. The most straightforward is to assume that the volume of the cave formed by erosion of tephra into the magma is equal to the volume of entrained tephra. The LiDAR data [LaFemina and Normandeau 2016] and measuring tools presented by Zhao et al. [2019] were used to estimate a cave volume of 4×10^4 m^3. For comparison, the volume of the Thríhnúkagígur composite cinder cone can be approximated assuming a conical shape with a radius of ~40 m and a height of 30 m, yielding a volume of 5.0×10^4 m^3. The area covered by the 3.5 ka lava flow is 3.5×10^5 m^2. Assuming the lava flow has an average thickness of one meter, yields an estimated to-

tal eruptive volume of approximately 4×10^5 m^3, likely within a factor of two. We treat the volume of the cave as a minimum estimate of tephra entrainment. With these assumptions and volume estimates, the erupted products are roughly 10 % entrained tephra by volume. The volume of material excavated by the erupting magma could be larger and more extensively filled in with lava drainback beneath the rockfall. However, given the relatively small eruptive volume, we conservatively assume the cave volume approximates the actual entrained volume of material. This 10 % estimate is close to the petrologic estimate of 4–8 % observed in thin sections of the lavas. We also note that tephra entrainment must have been a rapid process. Eruption timescales are estimated using magma flux rates (~3.8–13 m^3 s^{-1}) erupted during the Fagradsfjall eruption [Gudmundsson et al. 2021; Pedersen et al. 2021], which at the lowest end could produce the entire estimated eruptive volume in ~24 hours. With eruptive fluxes of 4.5 m^3 s^{-1}, ~0.5 m^3 of tephra would have been entrained per second on average. Regardless of the precise proportion, this extent of crustal entrainment is 2–4 orders of magnitude greater for these microxenoliths than noted for macro-scale crustal xenoliths in other monogenetic eruptions [Valentine and Groves 1996; Valentine 2012].

A primary observation of this study is the spatial correlation of the physical erosion of the tephra and the main cone of Thríhnúkagígur, which we also suggest is a causal relationship. Petrographic evidence of tephra entrainment in the Miðhnúkur lava sample and its co-location with Thríhnúkagígur further support this hypothesis. It is well accepted that pre-existing weaknesses in the crust can facilitate repeated eruption and vent construction in a particular location [Valentine and Krogh 2006; Maccaferri et al. 2010; Corvec et al. 2013]. For instance, lava was extruded through older craters during 2014–2015 Holuhraun eruption in the Barðarbunga system [Ruch et al. 2016]. While a causal relationship between location of the tephra cone at depth and the Miðhnúkur and Thríhnúkagígur spatter cones at the surface cannot be definitively proven, we posit that 1) the tephra at depth was an asperity that ascending magma could exploit, repeatedly, in two different fissure eruptions, and 2) the tephra focused magma flow and conduit development at these eruptive centers rather than elsewhere along the fissure. This is notably shallower than the depths of other syn-eruptively emplaced intrusion [Pederson et al. 2002; Díez et al. 2009; Kiyosugi et al. 2012] and highlights that structural or rheological contrasts even in the shallowest levels of the crust may impact eruptive dynamics. In the following sections, we explore the geochemical signatures of the buried tephra, feeder dike and lavas and investigate whether we can estimate the volume of entrained tephra using a geochemical mixing model.

5.2 Comparison to Reykjanes Peninsula basalts

Major element compositions of Thríhnúkagígur dikes and lavas are comparable to other Reykjanes Peninsula basalts. The tephra, while comparable to the dikes and lavas in terms of SiO$_2$ wt.%, extends to more enriched or more evolved compositions, with higher TiO$_2$, K$_2$O, and P$_2$O$_5$ at a given MgO. Such enrichment could partially be a result of fractional crys-

tallization of olivine and plagioclase from a similar parental liquid, which is supported by slightly lower MgO, CaO, and Al_2O_3 in the tephra. Incompatible trace element concentrations in the buried tephra are higher than in the most enriched historical Reykjanes Peninsula, which are also from Brennisteinsfjöll [Peate et al. 2009]. Geochemical enrichment may be more common in the Brennisteinsfjöll system because the crust is thicker here than the western Reykjanes Peninsula [Weir et al. 2001], which may facilitate crustal assimilation and fractional crystallization [Gee et al. 1998]. The tephra compositions could also represent undiluted fractional melts from a more enriched component in the mantle. These compositions are not, however, as enriched as some of the lavas erupted in the recent Fagradalsfjall eruption where compositions of up to 0.31 wt.% K_2O and La/Sm ratios of 3.05 were reported [Marshall et al. 2021], which were likely supplied directly from the mantle [Bali et al. 2021]. The tephra exposed in the cave at Thríhnúkagígur has equally high K_2O, but lower La/Sm ratios (maximum of 2.65).

In terms of radiogenic isotope ratios, $^{87}Sr/^{86}Sr$ and $^{143}Nd/^{144}Nd$ ratios for Thríhnúkagígur partially overlap with previously reported ratios for samples from Brennisteinsfjöll, and other volcanic systems on the Reykjanes Peninsula (i.e. Reykjanes and Krísuvík). They also overlap with lavas in the South Iceland Seismic Zone and the southern extent of the Eastern Volcanic Zone including Hekla, Katla, and Vestmannaeyjar [Park 1990; Furman et al. 1991; Sigmarsson et al. 1992; Furman et al. 1995; Thirlwall et al. 2004; Kokfelt 2006; Peate et al. 2009]. The dike samples are most comparable to previously reported values for Brennisteinsfjöll. Both lavas and buried tephra extend to more radiogenic values of $^{87}Sr/^{86}Sr$, consistent with some previous observations at Krísuvík [Gee et al. 1998] interpreted to reflect incorporation of crust altered by seawater [Marks et al. 2010; 2015].

Although the compositional range within the Thríhnúkagígur sample set is not large, it is worth considering the observed variations in the context of the near-surface magma plumbing system. The first-order observation is that the Thríhnúkagígur eruption cross cuts an older tephra cone just beneath the surface. The older tephra is geochemically distinct from the Thríhnúkagígur dikes and lavas, with greater enrichment in incompatible major and trace elements, and to a lesser degree in radiogenic isotopes. A circular intrusion is observed in the roof of the cave (Figure 6C), and a float sample believed to have been derived from that intrusion is distinguished by higher MgO and lower incompatible element abundances. The chilled dike margin has higher SiO_2 and lower incompatible trace elements compared to other dike samples. These subtle, yet distinct, variations in magma composition suggest reuse of the shallow conduit system by magmas that may initially have been derived from the same or a similar source but were stored separately prior to eruption. Assembly and incomplete mixing of diverse melts resulting in heterogeneity within a single eruption is not a novel observation in basaltic fissure eruptions in Iceland. For example, the 1973 eruption of Eldfell, had large variations in major element compositions through time [Furman et al. 1991]. Similarly, whole rock and melt inclusion incompatible trace

element data from a single basaltic lava flow at Borgarhraun record incomplete mixing of diverse melts [Maclennan et al. 2003]. Most recently, the 2021 Fagradalsfjall eruption similarly records a diversity of whole rock compositions including some with major element compositions that are unusually alkalic for Reykjanes Peninsula basalts and more similar to off-rift basalts in Iceland [Marshall et al. 2021]. Altogether, this suggests that variations in the dike and lava chemistry at Thríhnúkagígur are most plausibly related to deeper magmatic and melting processes rather than shallow microxenolith entrainment, despite observation of this process in the shallow conduit. Despite the geochemical complexity in Thríhnúkar magmas and eruptive products, we investigate the effect of tephra entrainment on lava chemistry in the following section.

5.3 Evaluating the effect of tephra entrainment on bulk lava geochemistry

Crustal contributions to magma genesis are commonly deduced from trace element and isotopic mixing trends [e.g. DePaolo 1981]. In the case of assimilation of basaltic crust by basaltic magma, the compositional impacts may be difficult to trace; for example, resulting in light stable isotope variation but little change in major or incompatible trace elements [Bindeman et al. 2008; Brounce et al. 2012]. At Thríhnúkagígur, we directly observe the entrainment of basaltic crustal materials into the erupted lavas. The question is, can we see evidence for this entrainment in the lava geochemistry? Given our conceptual model of conduit development and tephra entrainment, portions of the dike system, like the chilled margin of the dike, may best represent the pre-entrainment composition of the Thríhnúkagígur magma. Indeed, the multielement diagram (Figure 11) shows that the erupted lavas have trace element concentrations intermediate to those of the dikes and tephra, consistent with contamination of the dike magma by a small amount of incorporated tephra. However, the variability of estimates for tephra mixing for different trace elements or elemental ratios *within* a single sample are greater than the total variability of estimates for any given trace element or ratio *between* sample types, making it difficult to identify appropriate endmembers and to yield consistent results in mixing models. For instance, if we confine our mixing models to refractory trace element ratios (e.g. Nb/Zr vs. La/Yb) and take as the endmembers the chilled dike margin (TNG-27e) and an average tephra composition, the erupted lava compositions (and other dike compositions) are consistent with ~10–20 % tephra incorporation (Figure 14A). The chilled margin is perhaps the best candidate for magma involved at the onset of the intrusive-eruptive event before becoming contaminated with entrained tephra. However, mixing models using incompatible and mobile lithophile elements, such as Ba and Sr, require as much as 40–70 % tephra to account for the range of erupted lava compositions on a plot of Ba/La vs. Sr/Nd (Figure 14B). If the dike margin sample is excluded, however, we find almost complete overlap between the remaining dike samples and the lavas in this compositional space.

The overlap in radiogenic isotope ratios between the three sample types (i.e. dikes, lavas, and buried tephra) is such that there are no clear end-members or mixing trends. Thus, the
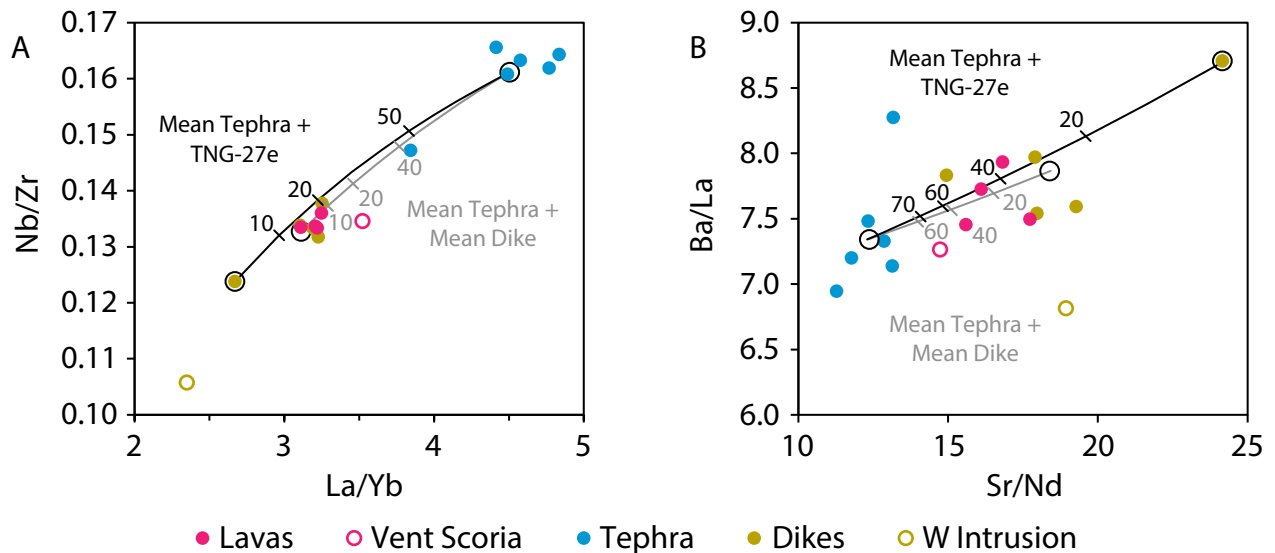
Figure 14: Trace element mixing curves between the mean tephra composition and two possible end members for the ascending magma—the chilled margin of the dike (TNG-27e) and the mean composition of the dike (which excludes the western wall intrusion). Estimates for the proportion of tephra in the erupted lavas varies greatly between different trace elements. Some more refractory elements (Nb/Zr vs La/Yb) yield lower estimates of 10–20 % tephra [A] while other lithophile elements (Ba/La vs Sr/Nd) yield higher estimates of 40–70 % tephra for some samples [B]. These large and nonsystematic differences suggest that other processes besides tephra incorporation into the magma must explain variation in Thríhnúkagígur geochemistry.

case for a chemical record of crustal assimilation is inconclusive in terms of incompatible trace elements and radiogenic isotope ratios. However, we observe some subtle trends in Sr and Nd isotopes, and these variations are roughly correlated with SiO_2 and MgO contents. This may be indicative that dikes, lavas, and tephra all have a similar parental magma, and the tephra are variably evolved by a slight amount of crustal assimilation [Gee et al. 1998]. If we did not know observationally that tephra entrainment and incorporation into the lavas occurred, we would not deduce it from this geochemical data set. This result, or lack thereof, suggests that crustal contamination in dominantly basaltic systems like Iceland may be more pervasive than currently recognized. Although this cryptic process will have little bearing on geochemical interpretations of magmatic processes, this result highlights the need to consider the thermo-mechanical erosion of crust during magma transport and storage in the crust.

6 CONCLUSIONS

The cave that formed within the shallow plumbing system at Thríhnúkagígur provides unique insight to the process of conduit formation during basaltic fissure eruptions and monogenetic basaltic eruptions more broadly. Intersection and entrainment of a large tephra unit by an ascending dike directly below Thríhnúkagígur focused magma flow preferentially to this location as opposed to other vents along the fissure. We posit that the three eruptive vents that make up the Thríhnúkar system (i.e. Thríhnúkagígur, Miðhnúkur, and Vesturhnúkur) are co-located because tephra and hyaloclastite form a low-density, poorly consolidated layer in the shallow subsurface that serves to focus magma rising in the dike

swarm at this location. Indeed, the lava from Miðhnúkur also contains the clusters of tephra shards (Figure 7E) observed in the Thríhnúkagígur lavas and suggest that this unit of unconsolidated material at depth has helped focus magma flow at the same location during multiple eruptive events. These observations reinforce previous studies that demonstrate lithological and structural heterogeneities in [Valentine and Krogh 2006; Maccaferri et al. 2010; Corvec et al. 2013]. Further, the approximate depths of tephra entrainment between 100 and 200 m are notably shallower than previously documented for any such crustal structural controls on eruption dynamics.

Thríhnúkagígur is exceptional in that a significant quantity of microxenolithic material (~10 % by volume) was entrained into the ascending magma, and one-of-a-kind in that the source of this scoured material is accessible for direct observation in a cave system directly underlying the vent. Elsewhere in Iceland, a similar proportion of assimilated hydrothermally altered crust has been invoked to explain O, B, and Sr isotope ratios in pristine basalts and melt inclusions [Gee et al. 1998; Bindeman et al. 2008; Brounce et al. 2012; Hampton et al. 2021]. Thríhnúkagígur highlights the challenges to identifying cryptic crustal contamination of basaltic magmas as the tephra and dike end-member compositions are insufficiently distinct from one another to produce clear mixing trends in the erupted lava compositions, even though entrained tephra is observed in thin section. To have an observable impact on lava geochemistry, extreme values in the assimilant may be required—for instance, highly fractionated stable isotope ratios in hydrothermally altered crust. The involvement of multiple small batches of magma in the early stages of eruption, ultimately giving way to a compositionally homogeneous magma flux at the peak of eruption, is more

likely to dominate geochemical heterogeneity observed in the Thríhnúkagígur dike system.

DATA AVAILABILITY

Petrographic data (Table S1) and geochemical data (Table S2) are provided in the Harvard Dataverse Repository at `https://doi.org/10.7910/DVN/MJYCDP` [Hudak et al. 2022].

REFERENCES

Árnadóttir, T., W. Jiang, K. L. Feigl, H. Geirsson, and E. Sturkell (2006). "Kinematic models of plate boundary deformation in southwest Iceland derived from GPS observations". *Journal of Geophysical Research* 111(B7). DOI: `10.1029/2005jb003907`.

Bali, E., A. Caracciolo, G. Gudfinnsson, E. Marshall, M. Bar Rasmussen, S. Matthews, E. Ranta, G. Mibei, and S. Halldorsson (2021). "Melt Transport Directly from the Mantle During the Fagradalsfjall Eruption, Iceland". In: *AGU Fall Meeting Abstracts*. Volume 2021, V12B-07, V12B–07.

Bindeman, I., A. Gurenko, O. Sigmarsson, and M. Chaussidon (2008). "Oxygen isotope heterogeneity and disequilibria of olivine crystals in large volume Holocene basalts from Ice-land: Evidence for magmatic digestion and erosion of Pleistocene hyaloclastites". *Geochimica et Cosmochimica Acta* 72(17), pages 4397–4420. DOI: `10.1016/j.gca.2008.06.010`.

Brounce, M., M. Feineman, P. LaFemina, and A. Gurenko (2012). "Insights into crustal assimilation by Icelandic basalts from boron isotopes in melt inclusions from the 1783–1784 Lakagígar eruption". *Geochimica et Cosmochimica Acta* 94, pages 164–180. DOI: `10.1016/j.gca.2012.07.002`.

Brown, R., J. Kavanagh, R. Sparks, M. Tait, and M. Field (2007). "Mechanically disrupted and chemically weakened zones in segmented dike systems cause vent localization: Evidence from kimberlite volcanic systems". *Geology* 35(9), page 815. DOI: `10.1130/g23670a.1`.

Bruce, P. M. and H. E. Huppert (1989). "Thermal control of basaltic fissure eruptions". *Nature* 342(6250), pages 665–667. DOI: `10.1038/342665a0`.

Cannaò, E., S. Agostini, M. Scambelluri, S. Tonarini, and M. Godard (2015). "B, Sr and Pb isotope geochemistry of high-pressure Alpine metaperidotites monitors fluid-mediated element recycling during serpentinite dehydration in subduction mélange (Cima di Gagnone, Swiss Central Alps)". *Geochimica et Cosmochimica Acta* 163, pages 80–100. DOI: `10.1016/j.gca.2015.04.024`.

Carey, R. and B. Houghton (2010). ""Inheritance": An influence on the particle size of pyroclastic deposits". *Geology* 38(4), pages 347–350. DOI: `10.1130/g30573.1`.

Clifton, A. E. and S. A. Kattenhorn (2006). "Structural architecture of a highly oblique divergent plate boundary segment". *Tectonophysics* 419(1–4), pages 27–40. DOI: `10.1016/j.tecto.2006.03.016`.

Corvec, N. L., T. Menand, and J. Lindsay (2013). "Interaction of ascending magma with pre-existing crustal fractures in monogenetic basaltic volcanism: an experimental approach". *Journal of Geophysical Research: Solid Earth* 118(3), pages 968–984. DOI: `10.1002/jgrb.50142`.

Delaney, P. T. and D. D. Pollard (1981). *Deformation of host rocks and flow of magma during growth of minette dikes and breccia-bearing intrusions near Ship Rock, New Mexico*. `https://pubs.usgs.gov/pp/1202`. [US Geological Survey Professional Paper 1202].

DePaolo, D. J. (1981). "Trace element and isotopic effects of combined wallrock assimilation and fractional crystallization". *Earth and Planetary Science Letters* 53(2), pages 189–202. DOI: `10.1016/0012-821x(81)90153-9`.

Díez, M., C. Connor, S. Kruse, L. Connor, and I. Savov (2009). "Evidence of small-volume igneous diapirism in the shallow crust of the Colorado Plateau, San Rafael Desert, Utah". *Lithosphere* 1(6), pages 328–336. DOI: `10.1130/l61.1`.

Einarsson, P. and K. Sæmundsson (1987). "Earthquake epicenters 1982-1985 and volcanic systems in Iceland [*Upptok jardskjalfta 1982-1985 og eldstodvakerfi a Islandi*]". In: *I hlutarins eðli: Festschrift for Thorbjorn Sigurgeirsson*. Edited by Þ. Sigfússon. [Map scale 1:750 000; Text in English and Icelandic.]

Einarsson, P. (2008). "Plate boundaries, rifts and transforms in Iceland". *Jökull* 58(12), pages 35–58.

Furman, T., F. A. Frey, and K.-H. Park (1991). "Chemical constraints on the petrogenesis of mildly alkaline lavas from Vestmannaeyjar, Iceland: the Eldfell (1973) and Surtsey (1963–1967) eruptions". *Contributions to Mineralogy and Petrology* 109(1), pages 19–37. DOI: 10.1007/bf00687198.

– (1995). "The scale of source heterogeneity beneath the Eastern neovolcanic zone, Iceland". *Journal of the Geological Society* 152(6), pages 997–1002. DOI: 10.1144/gsl.jgs.1995.152.01.20.

Gansecki, C., R. L. Lee, T. Shea, S. P. Lundblad, K. Hon, and C. Parcheta (2019). "The tangled tale of Kīlauea's 2018 eruption as told by geochemical monitoring". *Science* 366(6470). DOI: 10.1126/science.aaz0147.

Gee, M. A. M., R. N. Taylor, M. F. Thirlwall, and B. J. Murton (2000). "Axial magma reservoirs located by variation in lava chemistry along Iceland's mid-ocean ridge". *Geology* 28(8), pages 699–702. DOI: 10.1130/0091-7613(2000)28<699:amrlbv>2.0.co;2.

Gee, M. A. M., M. F. Thirlwall, R. N. Taylor, D. Lowry, and B. J. Murton (1998). "Crustal Processes: Major Controls on Reykjanes Peninsula Lava Chemistry, SW Iceland". *Journal of Petrology* 39(5), pages 819–839. DOI: 10.1093/petroj/39.5.819.

Genareau, K., G. A. Valentine, G. Moore, and R. L. Hervig (2010). "Mechanisms for transition in eruptive style at a monogenetic scoria cone revealed by microtextural analyses (Lathrop Wells volcano, Nevada, U.S.A.)" *Bulletin of Volcanology* 72(5), pages 593–607. DOI: 10.1007/s00445-010-0345-z.

Geshi, N. and M. Neri (2014). "Dynamic feeder dyke systems in basaltic volcanoes: the exceptional example of the 1809 Etna eruption (Italy)". *Frontiers in Earth Science* 2. DOI: 10.3389/feart.2014.00013.

Gudmundsson, A., M. Bazargan, A. Hobe, B. Selek, and A. Tryggvason (2021). "Dike-Segment Propagation, Arrest, and Eruption at Fagradalsfjall, Iceland". In: *AGU Fall Meeting Abstracts*. Volume 2021, V21A-08, V21A–08.

Gudmundsson, A. and I. F. Loetveit (2005). "Dyke emplacement in a layered and faulted rift zone". *Journal of Volcanology and Geothermal Research* 144(1–4), pages 311–327. DOI: 10.1016/j.jvolgeores.2004.11.027.

Gudmundsson, M. T., K. Jónsdóttir, A. Hooper, E. P. Holohan, S. A. Halldórsson, B. G. Ófeigsson, S. Cesca, K. S. Vogfjörd, F. Sigmundsson, T. Högnadóttir, P. Einarsson, O. Sigmarsson, A. H. Jarosch, K. Jónasson, E. Magnússon, S. Hreinsdóttir, M. Bagnardi, M. M. Parks, V. Hjörleifsdóttir, F. Pálsson, T. R. Walter, M. P. J. Schöpfer, S. Heimann, H. I. Reynolds, S. Dumont, E. Bali, G. H. Gudfinnsson, T. Dahm, M. J. Roberts, M. Hensch, J. M. C. Belart, K. Spaans, S. Jakobsson, G. B. Gudmundsson, H. M. Fridriksdóttir, V. Drouin, T. Dürig, G. Aðalgeirsdóttir, M. S. Riishuus, G. B. M. Pedersen, T. van Boeckel, B. Oddsson, M. A. Pfeffer, S. Barsotti, B. Bergsson, A. Donovan, M. R. Burton, and A. Aiuppa (2016). "Gradual caldera collapse at Bárdarbunga volcano, Iceland, regulated by lateral magma outflow". *Science* 353(6296). DOI: 10.1126/science.aaf8988.

Hampton, R., I. Bindeman, R. Stern, M. Coble, and S. Rooyakkers (2021). "A microanalytical oxygen isotopic and U-Th geochronologic investigation and modeling of rhyolite petrogenesis at the Krafla Central Volcano, Iceland". *Journal of Volcanology and Geothermal Research* 414, page 107229. DOI: 10.1016/j.jvolgeores.2021.107229.

Harp, A. G. and G. A. Valentine (2015). "Shallow plumbing and eruptive processes of a scoria cone built on steep terrain". *Journal of Volcanology and Geothermal Research* 294, pages 37–55. DOI: 10.1016/j.jvolgeores.2015.02.008.

Hintz, A. R. and G. A. Valentine (2012). "Complex plumbing of monogenetic scoria cones: New insights from the Lunar Crater Volcanic Field (Nevada, USA)". *Journal of Volcanology and Geothermal Research* 239–240, pages 19–32. DOI: 10.1016/j.jvolgeores.2012.06.008.

Houghton, B. F., C. M. Tisdale, E. W. Llewellin, J. Taddeucci, T. R. Orr, B. Walker, and M. R. Patrick (2021). "The Birth of a Hawaiian Fissure Eruption". *Journal of Geophysical Research: Solid Earth* 126(1). DOI: 10.1029/2020jb020903.

Hudak, M. R., M. D. Feineman, P. C. LaFemina, H. Geirsson, and S. Agostini (2022). *Data for "Conduit formation and crustal microxenolith entrainment in a basaltic fissure eruption: Observations from Thríhnúkagígur Volcano, Iceland"*. https://doi.org/10.7910/DVN/MJYCDP. [dataset].

Hughes, S. S., S. E. Kobs Nawotniak, D. W. Sears, C. Borg, W. B. Garry, E. H. Christiansen, C. W. Haberle, D. S. Lim, and J. L. Heldmann (2018). "Phreatic explosions during basaltic fissure eruptions: Kings Bowl lava field, Snake River Plain, USA". *Journal of Volcanology and Geothermal Research* 351, pages 89–104. DOI: 10.1016/j.jvolgeores.2018.01.001.

Jakobsson, S. P., J. Jónsson, and F. Shido (1978). "Petrology of the Western Reykjanes Peninsula, Iceland". *Journal of Petrology* 19(4), pages 669–705. DOI: 10.1093/petrology/19.4.669.

Jochum, K. P., U. Nohl, K. Herwig, E. Lammel, B. Stoll, and A. W. Hofmann (2005). "GeoReM: A New Geochemical Database for Reference Materials and Isotopic Standards". *Geostandards and Geoanalytical Research* 29(3), pages 333–338. DOI: 10.1111/j.1751-908x.2005.tb00904.x.

Jones, T. J., B. F. Houghton, E. W. Llewellin, C. E. Parcheta, and L. Höltgen (2018). "Spatter matters – distinguishing primary (eruptive) and secondary (non-eruptive) spatter deposits". *Scientific Reports* 8(1). DOI: 10.1038/s41598-018-27065-1.

Jones, T. J., E. W. Llewellin, B. F. Houghton, R. J. Brown, and C. Vye-Brown (2017). "Proximal lava drainage controls on basaltic fissure eruption dynamics". *Bulletin of Volcanology* 79(11). DOI: 10.1007/s00445-017-1164-2.

Keating, G. N., G. A. Valentine, D. J. Krier, and F. V. Perry (2008). "Shallow plumbing systems for small-volume basaltic volcanoes". *Bulletin of Volcanology* 70(5), pages 563–582. DOI: 10.1007/s00445-007-0154-1.

Kelley, K. A., T. Plank, J. Ludden, and H. Staudigel (2003). "Composition of altered oceanic crust at ODP Sites 801 and 1149". *Geochemistry, Geophysics, Geosystems* 4(6), n/a–n/a. DOI: 10.1029/2002gc000435.

Kiyosugi, K., C. B. Connor, P. H. Wetmore, B. P. Ferwerda, A. M. Germa, L. J. Connor, and A. R. Hintz (2012). "Relationship between dike and volcanic conduit distribution in a highly eroded monogenetic volcanic field: San Rafael, Utah, USA". *Geology* 40(8), pages 695–698. DOI: 10.1130/g33074.1.

Kokfelt, T. F. (2006). "Combined Trace Element and Pb-Nd-Sr-O Isotope Evidence for Recycled Oceanic Crust (Upper and Lower) in the Iceland Mantle Plume". *Journal of Petrology* 47(9), pages 1705–1749. DOI: 10.1093/petrology/egl025.

Koornneef, J. M., A. Stracke, B. Bourdon, M. A. Meier, K. P. Jochum, B. Stoll, and K. Grönvold (2012). "Melting of a Two-component Source beneath Iceland". *Journal of Petrology* 53(1), pages 127–157. DOI: 10.1093/petrology/egr059.

LaFemina, P. and J. Normandeau (2016). *Thrihnukagigur Volcano Conduit Mapping TLS*. https://doi.org/10.7283/R3RP41. DOI: 10.7283/R3RP41. [dataset].

Lefebvre, N., J. White, and B. Kjarsgaard (2012). "Spatter-dike reveals subterranean magma diversions: Consequences for small multivent basaltic eruptions". *Geology* 40(5), pages 423–426. DOI: 10.1130/g32794.1.

Maccaferri, F., M. Bonafede, and E. Rivalta (2010). "A numerical model of dyke propagation in layered elastic media". *Geophysical Journal International* 180(3), pages 1107–1123. DOI: 10.1111/j.1365-246x.2009.04495.x.

Macedonio, G., F. Dobran, and A. Neri (1994). "Erosion processes in volcanic conduits and application to the AD 79 eruption of Vesuvius". *Earth and Planetary Science Letters* 121(1-2), pages 137–152. DOI: 10.1016/0012-821x(94)90037-x.

Maclennan, J., D. McKenzie, F. Hilton, K. Gronvöld, and N. Shimizu (2003). "Geochemical variability in a single flow from northern Iceland". *Journal of Geophysical Research: Solid Earth* 108(B1), ECV 4–1–ECV 4–21. DOI: 10.1029/2000jb000142.

Marks, N., P. Schiffman, R. A. Zierenberg, H. Franzson, and G. Ó. Fridleifsson (2010). "Hydrothermal alteration in the Reykjanes geothermal system: Insights from Iceland deep drilling program well RN-17". *Journal of Volcanology and Geothermal Research* 189(1-2), pages 172–190. DOI: 10.1016/j.jvolgeores.2009.10.018.

Marks, N., R. A. Zierenberg, and P. Schiffman (2015). "Strontium and oxygen isotopic profiles through 3 km of hydrothermally altered oceanic crust in the Reykjanes Geothermal System, Iceland". *Chemical Geology* 412, pages 34–47. DOI: 10.1016/j.chemgeo.2015.07.006.

Marshall, E., M. Bar Rasmussen, S. Halldorsson, S. Matthews, E. Ranta, O. Sigmarsson, J. Gunnarsson Robin, E. Bali, A. Caracciolo, G. Gudfinnsson, and G. Mibei (2021). "Rapid geochemical evolution of the mantle-sourced Fagradalsfjall eruption, Iceland". In: *AGU Fall Meeting Abstracts*. Volume 2021, V14B-06, V14B–06.

Mastin, L. G. and M. S. Ghiorso (2000). *A numerical program for steady-state flow of magma-gas mixtures through vertical eruptive conduits*. https://pubs.usgs.gov/of/2000/0209/. [US Geological Survey Open-File Report 00-209] (vers. 1.05b, April 2008).

Mitchell, K. L. (2005). "Coupled conduit flow and shape in explosive volcanic eruptions". *Journal of Volcanology and Geothermal Research* 143(1-3), pages 187–203. DOI: 10.1016/j.jvolgeores.2004.09.017.

Muirhead, J. D., A. R. V. Eaton, G. Re, J. D. L. White, and M. H. Ort (2016). "Monogenetic volcanoes fed by interconnected dikes and sills in the Hopi Buttes volcanic field, Navajo Nation, USA". *Bulletin of Volcanology* 78(2). DOI: 10.1007/s00445-016-1005-8.

Neal, C. A., S. R. Brantley, L. Antolik, J. L. Babb, M. Burgess, K. Calles, M. Cappos, J. C. Chang, S. Conway, L. Desmither, P. Dotray, T. Elias, P. Fukunaga, S. Fuke, I. A. Johanson, K. Kamibayashi, J. Kauahikaua, R. L. Lee, S. Pekalib, A. Miklius, W. Million, C. J. Moniz, P. A. Nadeau, P. Okubo, C. Parcheta, M. R. Patrick, B. Shiro, D. A. Swanson, W. Tollett, F. Trusdell, E. F. Younger, M. H. Zoeller, E. K. Montgomery-Brown, K. R. Anderson, M. P. Poland, J. L. Ball, J. Bard, M. Coombs, H. R. Dietterich, C. Kern, W. A. Thelen, P. F. Cervelli, T. Orr, B. F. Houghton, C. Gansecki, R. Hazlett, P. Lundgren, A. K. Diefenbach, A. H. Lerner, G. Waite, P. Kelly, L. Clor, C. Werner, K. Mulliken, G. Fisher, and D. Damby (2019). "The 2018 rift eruption and summit collapse of Kīlauea Volcano". *Science* 363(6425), pages 367–374. DOI: 10.1126/science.aav7046.

Németh, K. and G. Kereszturi (2015). "Monogenetic volcanism: personal views and discussion". *International Journal of Earth Sciences* 104(8), pages 2131–2146. DOI: 10.1007/s00531-015-1243-6.

Németh, K. and J. D. White (2003). "Reconstructing eruption processes of a Miocene monogenetic volcanic field from vent remnants: Waipiata Volcanic Field, South Island, New Zealand". *Journal of Volcanology and Geothermal Research* 124(1-2), pages 1–21. DOI: 10.1016/s0377-0273(03)00042-8.

Nicholson, H., M. Condomines, J. G. Fitton, A. E. Fallick, K. Grönvold, and G. Rogers (1991). "Geochemical and Isotopic Evidence for Crustal Assimilation Beneath Krafla, Iceland". *Journal of Petrology* 32(5), pages 1005–1020. DOI: 10.1093/petrology/32.5.1005.

Orr, T. R., J. E. Bleacher, M. R. Patrick, and K. M. Wooten (2015). "A sinuous tumulus over an active lava tube at Kīlauea Volcano: Evolution, analogs, and hazard forecasts". *Journal of Volcanology and Geothermal Research* 291, pages 35–48. DOI: 10.1016/j.jvolgeores.2014.12.002.

Parcheta, C. E., B. F. Houghton, and D. A. Swanson (2012). "Hawaiian fissure fountains 1: decoding deposits—episode 1 of the 1969–1974 Mauna Ulu eruption". *Bulletin of Volcanology* 74(7), pages 1729–1743. DOI: 10.1007/s00445-012-0621-1.

Park, K.-H. (1990). "Sr, Nd and Pb isotope studies of ocean island basalts: Constraints on their origin and evolution". PhD thesis. Columbia University New York.

Patrick, M. R., K. R. Anderson, M. P. Poland, T. R. Orr, and D. A. Swanson (2015). "Lava lake level as a gauge of magma reservoir pressure and eruptive hazard". *Geology* 43(9), pages 831–834. DOI: 10.1130/g36896.1.

Patrick, M. R. and T. R. Orr (2012). "Rootless shield and perched lava pond collapses at Kīlauea Volcano, Hawai'i". *Bulletin of Volcanology* 74(1), pages 67–78. DOI: 10.1007/s00445-011-0505-9.

Peate, D. W., J. A. Baker, S. P. Jakobsson, T. E. Waight, A. J. R. Kent, N. V. Grassineau, and A. C. Skovgaard (2009). "Historic magmatism on the Reykjanes Peninsula, Iceland: a snap-shot of melt generation at a ridge segment". *Contributions to Mineralogy and Petrology* 157(3), pages 359–382. DOI: 10.1007/s00410-008-0339-4.

Pedersen, G., A. Höskuldsson, T. Dürig, T. Thordarson, I. Jónsdóttir, M. Riishuus, B. Óskarsson, S. Dumont, E. Magnusson, M. Gudmundsson, F. Sigmundsson, V. Drouin, C. Gallagher, R. Askew, J. Gudnason, W. Moreland, P. Nikkola, H. Reynolds, and J. Schmith (2017). "Lava field evolution and emplacement dynamics of the 2014–2015 basaltic fissure eruption at Holuhraun, Iceland". *Journal of Volcanology and Geothermal Research* 340, pages 155–169. DOI: 10.1016/j.jvolgeores.2017.02.027.

Pedersen, G., M. Gudmundsson, B. Oskarsson, J. Berlart, N. Gies, T. Hognadottir, A. R. Hjartardottir, T. Durig, H. Reynolds, G. Valsson, C. Hamilton, A. Gunnarsson, V. Pinel, E. Berthier, P. Einarsson, and B. Oddsson (2021). "Volume, Discharge Rate and Lava Transport at the Fagradalsfjall Eruption 2021: Results from Near-Real Time Photogrammetric Monitoring". In: *AGU Fall Meeting Abstracts*. Volume 2021, V35F-01, V35F–01.

Pederson, J. L., R. D. Mackley, and J. L. Eddleman (2002). "Colorado Plateau uplift and erosion evaluated using GIS". *GSA Today* 12(8), pages 4–10.

Peterson, D. W., R. T. Holcomb, R. I. Tilling, and R. L. Christiansen (1994). "Development of lava tubes in the light of observations at Mauna Ulu, Kilauea Volcano, Hawaii". *Bulletin of Volcanology* 56(5), pages 343–360. DOI: 10.1007/bf00326461.

Pollard, D. D., O. H. Muller, and D. R. Dockstader (1975). "The Form and Growth of Fingered Sheet Intrusions". *Geological Society of America Bulletin* 86(3), page 351. DOI: 10.1130/0016-7606(1975)86<351:tfagof>2.0.co;2.

Richardson, J., C. Connor, P. Wetmore, L. Connor, and E. Gallant (2015). "Role of sills in the development of volcanic fields: Insights from lidar mapping surveys of the San Rafael Swell, Utah". *Geology* 43(11), pages 1023–1026. DOI: 10.1130/g37094.1.

Richter, D., J. Eaton, K. Murata, W. Ault, and H. Krivoy (1970). *Chronological narrative of the 1959-60 eruption of Kilauea Volcano, Hawaii.* DOI: 10.3133/pp537e. [US Geological Survey Professional Paper 537-E].

Roman, D. C. and K. V. Cashman (2006). "The origin of volcano-tectonic earthquake swarms". *Geology* 34(6), page 457. DOI: 10.1130/g22269.1.

Rubin, A. M. (1995). "Propagation of magma-filled cracks". *Annual Review of Earth and Planetary Sciences* 23, pages 287–336. DOI: 10.1146/annurev.ea.23.050195.001443.

Ruch, J., T. Wang, W. Xu, M. Hensch, and S. Jónsson (2016). "Oblique rift opening revealed by reoccurring magma injection in central Iceland". *Nature Communications* 7(1). DOI: 10.1038/ncomms12352.

Sæmundsson, K. (2006). *Þríhnúkagígur: Jarðfræðirannsóknir og tillögur vegna gangagerðar* [Þríhnúkagígur: Geological studies and proposals for tunnel construction]. Report: ÍSOR-06144, Verknr: 500-078. [In Icelandic].

– (2008). *Þríhnúkagígur: Helstu niðurstöður kjarnaborana* [Þríhnúkagígur: Main results of drill cores]. Report: ÍSOR-08103, Verknr: 500-078. [In Icelandic].

Sæmundsson, K., H. Jóhannesson, Á. Hjartarson, S. G. Kristinsson, and M. Sigurgeirsson (2010). *Geological map of southwest Iceland.* [Scale: 1: 100,000].

Sæmundsson, K., M. Á. Sigurgeirsson, and G. Ó. Friðleifsson (2020). "Geology and structure of the Reykjanes volcanic system, Iceland". *Journal of Volcanology and Geothermal Research* 391, page 106501. DOI: 10.1016/j.jvolgeores.2018.11.022.

Sigmarsson, O., M. Condomines, and S. Fourcade (1992). "A detailed Th, Sr and O isotope study of Hekla: differentiation processes in an Icelandic Volcano". *Contributions to Mineralogy and Petrology* 112(1), pages 20–34. DOI: 10.1007/bf00310953.

Sigmundsson, F., A. Hooper, S. Hreinsdóttir, K. S. Vogfjörd, B. G. Ófeigsson, E. R. Heimisson, S. Dumont, M. Parks, K. Spaans, G. B. Gudmundsson, V. Drouin, T. Árnadóttir, K. Jónsdóttir, M. T. Gudmundsson, T. Högnadóttir, H. M. Fridriksdóttir, M. Hensch, P. Einarsson, E. Magnússon, S. Samsonov, B. Brandsdóttir, R. S. White, T. Ágústsdóttir, T. Greenfield, R. G. Green, Á. R. Hjartardóttir, R. Pedersen, R. A. Bennett, H. Geirsson, P. C. La Femina, H. Björnsson, F. Pálsson, E. Sturkell, C. J. Bean, M. Möllhoff, A. K. Braiden, and E. P. S. Eibl (2015). "Segmented lateral dyke growth in a rifting event at Bárðarbunga volcanic system, Iceland". *Nature* 517(7533), pages 191–195. DOI: 10.1038/nature14111.

Stefánsson, Á. B. (1992). "Þríhnúkagígur". *Náttúrufræðingurinn* 61, pages 229–242.

Stovall, W. K., B. F. Houghton, A. J. L. Harris, and D. A. Swanson (2009). "Features of lava lake filling and draining and their implications for eruption dynamics". *Bulletin of Volcanology* 71(7), pages 767–780. DOI: 10.1007/s00445-009-0263-0.

Sturkell, E., F. Sigmundsson, P. Einarsson, and R. Bilham (1994). "Strain accumulation 1986-1992 across the Reykjanes Peninsula Plate Boundary, Iceland, determined from GPS measurements". *Geophysical Research Letters* 21(2), pages 125–128. DOI: 10.1029/93gl03421.

Sun, S.-s. and W. F. McDonough (1989). "Chemical and isotopic systematics of oceanic basalts: implications for mantle composition and processes". *Geological Society, London, Special Publications* 42(1), pages 313–345. DOI: 10.1144/gsl.sp.1989.042.01.19.

Swanson, D. A., D. W A, J. D B, and P. D W (1979). *Chronological narrative of the 1969-71 Mauna Ulu eruption of Kilauea Volcano, Hawaii.* https://pubs.usgs.gov/pp/1056/. [US Geological Survey Professional Paper 1056].

Taylor, B., K. Crook, and J. Sinton (1994). "Extensional transform zones and oblique spreading centers". *Journal of Geophysical Research: Solid Earth* 99(B10), pages 19707–19718. DOI: 10.1029/94jb01662.

Thirlwall, M., M. Gee, R. Taylor, and B. Murton (2004). "Mantle components in Iceland and adjacent ridges investigated using double-spike Pb isotope ratios". *Geochimica et Cosmochimica Acta* 68(2), pages 361–386. DOI: 10.1016/s0016-7037(03)00424-1.

Thordarson, T. and G. Larsen (2007). "Volcanism in Iceland in historical time: Volcano types, eruption styles and eruptive history". *Journal of Geodynamics* 43(1), pages 118–152. DOI: 10.1016/j.jog.2006.09.005.

Townsend, M. R. (2018). "Modeling Thermal Pressurization Around Shallow Dikes Using Temperature-Dependent Hydraulic Properties: Implications for Deformation Around Intrusions". *Journal of Geophysical Research: Solid Earth* 123(1), pages 311–323. DOI: 10.1002/2017jb014455.

Townsend, M. R., D. D. Pollard, K. Johnson, and C. Culha (2015). "Jointing around magmatic dikes as a precursor to the development of volcanic plugs". *Bulletin of Volcanology* 77(10). DOI: 10.1007/s00445-015-0978-z.

Valentine, G. A. (2012). "Shallow plumbing systems for small-volume basaltic volcanoes, 2: Evidence from crustal xenoliths at scoria cones and maars". *Journal of Volcanology and Geothermal Research* 223-224, pages 47–63. DOI: 10.1016/j.jvolgeores.2012.01.012.

Valentine, G. A. and T. K. P. Gregg (2008). "Continental basaltic volcanoes — Processes and problems". *Journal of Volcanology and Geothermal Research* 177(4), pages 857–873. DOI: 10.1016/j.jvolgeores.2008.01.050.

Valentine, G. A. and K. R. Groves (1996). "Entrainment of country rock during basaltic eruptions of the Lucero volcanic field, New Mexico". *The Journal of Geology* 104(1), pages 71–90.

Valentine, G. A. and K. Krogh (2006). "Emplacement of shallow dikes and sills beneath a small basaltic volcanic center – The role of pre-existing structure (Paiute Ridge, southern Nevada, USA)". *Earth and Planetary Science Letters* 246(3–4), pages 217–230. DOI: 10.1016/j.epsl.2006.04.031.

Wadsworth, F. B., B. M. Kennedy, M. J. Branney, F. W. von Aulock, Y. Lavallée, and A. Menendez (2015). "Exhumed conduit records magma ascent and drain-back during a Strombolian eruption at Tongariro volcano, New Zealand". *Bulletin of Volcanology* 77(9). DOI: 10.1007/s00445-015-0962-7.

Weir, N. R. W., R. S. White, B. Brandsdóttir, P. Einarsson, H. Shimamura, and H. Shiobara (2001). "Crustal structure of the northern Reykjanes Ridge and Reykjanes Peninsula, southwest Iceland". *Journal of Geophysical Research: Solid Earth* 106(B4), pages 6347–6368. DOI: 10.1029/2000jb900358.

Whitehead, J. A. and K. R. Helfrich (1991). "Instability of flow with temperature-dependent viscosity: A model of magma dynamics". *Journal of Geophysical Research: Solid Earth* 96(B3), pages 4145–4155. DOI: 10.1029/90jb02342.

Wilson, L. and J. W. Head (1981). "Ascent and eruption of basaltic magma on the Earth and Moon". *Journal of Geophysical Research: Solid Earth* 86(B4), pages 2971–3001. DOI: 10.1029/jb086ib04p02971.

Wylie, J. J., K. R. Helfrich, B. Dade, J. R. Lister, and J. F. Salzig (1999). "Flow localization in fissure eruptions". *Bulletin of Volcanology* 60(6), pages 432–440. DOI: 10.1007/s004450050243.

Wylie, J. J. and J. R. Lister (1995). "The effects of temperature-dependent viscosity on flow in a cooled channel with application to basaltic fissure eruptions". *Journal of Fluid Mechanics* 305, pages 239–261. DOI: 10.1017/s0022112095004617.

Zhao, J., J. O. Wallgrün, P. C. LaFemina, J. Normandeau, and A. Klippel (2019). "Harnessing the power of immersive virtual reality - visualization and analysis of 3D earth science data sets". *Geo-spatial Information Science* 22(4), pages 237–250. DOI: 10.1080/10095020.2019.1621544.